Chemical Engineering Journal 479 (2024) 147927

Contents lists available at ScienceDirect

Chemical Engineering Journal

journal homepage: www.elsevier.com/locate/cej

Fischer-Tropsch synthesis to α-Olefins with low CO_2 selectivity on a Co_2C catalyst

Yiwen Liu [a], Chengyang He [a], Xingmao Jiang [a], Rui Zhang [a], Xinying Liu [b], Diane Hildebrandt [c], Xiaojun Lu [a,*]

[a] School of Chemical Engineering and Pharmacy and Key Laboratory for Green Chemical Process of Ministry of Education, Wuhan Institute of Technology, Wuhan 430205, China
[b] Institute for Catalysis and Energy Solutions, University of South Africa, c/o Christiaan de Wet & Pioneer, Florida 1709, Roodepoort, Gauteng, South Africa
[c] African Energy Leadership Centre and the School of Chemistry, University of the Witwatersrand, Johannesburg 2050, South Africa

ARTICLE INFO

Keywords:
Fischer-Tropsch to olefin
Lower olefins
Co_2C
Crystal facet
CO_2 selectivity

ABSTRACT

A Co_2C catalyst with low CO_2 selectivity for the Fischer-Tropsch to Olefins (FTO) was derived from a precursor catalyst prepared by a "melting" method. Co-Mn composite oxide, $MnCo_2O_{4.5}$, was identified as the dominant composition in the catalytic material before it was activated. The catalyst showed a weak interaction between Co and Mn with the presence of Na. Therefore, Co could be liberated easily from $MnCo_2O_{4.5}$ with H_2 reduction at a usually used condition for Co-based catalyst for the Fischer-Tropsch Synthesis (FTS). A clear carburization of Co^0 to Co_2C was observed during the initial period of reaction, and this transformation could be achieved within 6 h. Four different crystal facets, (210), (020), (111), and (101) for Co_2C, were identified once Co^0 has been successfully carburized during the reaction. A limited amount of Co^0 also transformed to Co_3O_4 during Co_2C formation when H_2O was produced by the FT reaction. The prepared catalyst demonstrated outstanding performance in terms of product selectivity. Its selectivity to lower olefins (C_2-C_4) was as high as 60.26 % with an average olefin/paraffin ratio of 26.69. Additional to high olefin selectivity, the CO_2 selectivity was as low as 11.49 %, and that of C_1 (CO_2 + CH_4) could be controlled at 16.44 % with optimal Co/Mn ratio and operating conditions. It was also found that transient state Co^0 with Mn and Na as promoters demonstrated similar high olefin to paraffin ratios when compared to Co_2C.

1. Introduction

Low-carbon olefins, referring as olefins with a carbon number less than five such as ethylene, propylene, butene, etc., are important essential intermediates in the chemical industry [1]. Conventionally, low-carbon olefins are mainly obtained from the steam cracking of naphtha. In the meantime, with the decreasing of petroleum resources, the conventional route in producing low-carbon olefins has yet to meet the demand, and there is an urgent need for non-petroleum processes to fulfill the vacancy [2–4]. Nowadays, the non-oil processes utilize syngas (a mixture of CO and H_2), deriving from carbon-containing resources such as coal, natural gas, and biomass, to produce low-carbon olefins directly or indirectly [5–7]. The indirect production of low-carbon olefins from syngas is mainly via the methanol conversion route, using CuZnAl [8] as the catalyst to convert syngas to methanol and then applying molecular sieve as the catalyst for MTO [9] (methanol to olefins) and MTP [10] (methanol to propylene) reactions. Large-scale MTO based on zeolite using a fluidized bed with circulating C_{4+} for the highly selective production of ethylene and propylene has been successfully commercialized [11].

Providing the availability of syngas, direct one-step production of low-carbon olefins with a shorter process can be economically more attractive than indirect production technologies because of less capital investment and energy consumption. Therefore, the direct production of olefins from syngas has received great attention. Researchers tend to prepare bifunctional catalysts with two components, coupling the methanol synthesis and olefin production by dehydration to simplify the process. The reaction activity of syngas to olefins at low temperatures is extremely low, so this type of bifunctional catalyst tends to adopt high pressure and temperature to increase the catalyst activity [12]. $ZnCrO_x$/SAPO-34 as a bifunctional catalyst for the direct conversion of syngas to low carbon olefin via OX-ZEO reaction was reported by Bao's group

* Corresponding author.
E-mail address: xiaojunlu@wit.edu.cn (X. Lu).

https://doi.org/10.1016/j.cej.2023.147927
Received 24 June 2023; Received in revised form 29 October 2023; Accepted 4 December 2023
Available online 6 December 2023

several years back, which facilitated C-O bond activation with metal oxides and C-C bond coupling by molecular sieves [13]. A high selectivity of 80 % for lower olefins was achieved at a CO conversation of 17 %. Subsequently, Wang and his colleagues reported a $ZnZrO_x$-SAPO-34 bifunctional catalyst by physical mixing, proposing coupling of reactions to control olefin selectivity by breaking the conventional Anderson-Schulz-Flory (ASF) distribution. A 75 % selectivity was achieved for C_2-C_4 olefins with 10 % CO conversion under 400 ℃ [14]. This catalytic process has the advantages of a shorter process and high selectivity to olefins. However, the high reaction temperature and low CO conversion may raise engineering challenges when scaled up to industrial capacities.

The direct conversion of syngas to low carbon olefins by the FTS reaction without any intermediate steps is known as the FTO process, and its product distribution normally follows the ASF distribution, i.e., the unwanted methane selectivity could be as high as about 30 %, while that of the C_2-C_4 products up to 60 % [15]. Although the ASF distribution hinders the selectivity to lower olefins from reaching a higher value further, the FTO also produces olefins with higher carbons numbers, such as C_5-C_9. It could therefore offer high value-added olefins for both C_2-C_4 and C_5-C_9 as long as the selectivity to CH_4 and other paraffins is at low levels. Fe- and Co-based catalysts are used for the FTO reaction due to their catalytic ability in CO dissociation, C-C coupling, and chain growth. To obtain a high selectivity to low-carbon olefins, the chain growth probability (α) of the catalyst should be controlled at a moderate level [16]. Fe-based catalysts have been widely studied due to its relatively weak hydrogenation ability and high olefin/paraffin (O/P) ratios in the products. de Jong's team utilized inert carriers to load Fe for the FTO process [17]. Fe nanoparticles were uniformly dispersed on α-alumina or carbon nanofiber, and the weak interaction between the carriers and the active Fe favored the formation of iron carbides, which resulted in up to 60 % of selectivity to low-carbon olefins. As the reaction was carried out at a higher temperature, carbon deposition was prone to occur, leading to catalyst deactivation and a short life span. Under the FTS reaction conditions, Fe-based catalysts are inclined to generate iron carbides with the induction of amorphous carbon or CO. However, iron carbides are easily oxidized and inactivated due to the presence of water formed by reactions. Recently, Ding and his colleagues designed a FeMn@Si-C catalyst with excellent hydrophobicity to prevent the adsorption of water molecules on the active Fe_xC_y sites [18]. The transformation of iron carbides to Fe_3O_4 was consequently inhibited, and CO_2 selectivity was reduced. At the same time, the electron transferring from an appropriate amount of Mn atoms to Fe promoted the dissociation of the adsorbed CO and accelerated the olefin production. The yield of olefins reached 36.6 % at a high CO conversion of 56.1 %, while the selectivity of the undesired C_1 products (CO_2 + CH_4) was controlled at 22.5 %. Li's team found that the stability of ε-Fe_2C could be significantly improved when replacing the amorphous carbon layer with a graphene shell to facilitate the carburization of α-Fe to form ε-Fe_2C [19]. The catalyst prepared by this method reached 95 % CO conversion at 300 °C, and the activity was stably maintained for at least 400 h.

Fe-based catalysts have rich active phases, and they offer abundant isomeric products. In contrast, Co-based catalysts for the FTS have higher selectivity to linear hydrocarbons (HCs) with higher activity and a longer life span. Usually, the metallic Co nanoparticles are the active sites in Co-based catalysts for the FT reaction, and the products are mainly paraffins with a limited quantity of olefins and chemicals such as alcohols [20,21]. The adsorbed H_2* and CO* species react on the Co surface to form surface CH_x species for further carbon–carbon coupling, which undergoes dehydrogenation and hydrogenation to form olefins and paraffins, respectively. The catalyst activity and product selectivity depend on the size of the Co nanoparticles, the nature of the carrier, the presence of promoters, the preparation method, and the pretreatment conditions [22]. The formation of methane and C_{5+} products could be adjusted by adding promoters. The alkali metal Na leads to a significant increase in CO adsorption [23], thus promoting the desorption of olefins. As an electronic promoter, it can also inhibit the secondary reactions of olefins from hydrogenation and isomerization, improving the selectivity of olefins. Mn could promote CO adsorption and increase the CO consumption rate by acting as Lewis acid to interact with the O atom of adsorbed CO [24]. The promoting effect of Mn also includes the influence on the distribution and exposure of active sites. The promoters modulate the surface electron environment of the active metal and lead to higher CO surface coverage, which is highly favorable for CO dissociation and C-C coupling while inhibiting methanation and chain termination triggered by the hydrogenation of alkyl species [25].

Zhong and his colleagues found that nano prisms Co_2C with the presence of Mn and Na demonstrated excellent catalytic performance in FTO and achieved high selectivity to lower olefins under mild reaction conditions (250 ℃, 0.1 MPa) [26]. Its lower olefin selectivity could reach 60.8 % based on all produced HCs, and the methane selectivity is controlled at about 5 %. The O/P ratio for C_2-C_4 was as high as 30, which means that around 97 % of C_2-C_4 HCs were olefinic products. However, this Co_2C catalyst also resulted in more than 40 % CO_2 selectivity, which is exceptionally high if one compares that to normal Co-based catalysts for the FTS. The kinetic study, characterization, and DFT calculations revealed that the active center, Co_2C, has a poor hydrogenation ability, and the exposed facets (1 0 1) and (0 2 0) favor olefin production. As an active phase for olefin production, Co_2C is often derived by the carburization of various Co-based precursor catalysts with the presence of syngas. However, it has long been believed that Co_2C generated in the FT reaction is an important cause of deactivation for Co-based catalysts, leading to higher CO_2 and CH_4 selectivity when compared to metallic Co [27]. According to Mohandas *et al.*, the formed Co_2C is not stable and could be transformed back to Co or Co_3O_4 under typical low-temperature FT conditions [28]. A recent study for Co_2C by *in situ* XAFS suggests that the Co_2C becomes unstable and gradually changes to metallic Co when increasing temperature from 250 ℃ to 280 ℃ [29]. This agrees with Ding's work [30] that Co_2C coexists with metallic Co at a similar temperature range. The catalytic performance of Co_2C also depends on the catalyst preparation method. Studies suggested that the co-precipitation method resulted in a better catalytic performance than the impregnation method in terms of selectivity to olefins and catalyst activity [31]. The conventional impregnation method to prepared Co_2C catalyst suffers from controlling Co nanoparticles to form a uniform dispersion on the complex internal surface of the supports and therefore results in poor performance with high selectivity to CO_2 and CH_4 [32]. Notably, Co_2C catalysts prepared by various methods reported in the literature [31] demonstrated high CO_2 selectivity in general, in order of 40 % based on the converted CO.

In this work, we report a Co-based catalyst prepared by the "melting" method, which manufactures uniform Co-Mn nanoparticles as the precursor catalyst. It shows a weak interaction between Co and Mn with the help from evenly dispersed Na, which is beneficial for the reduction to form metallic Co. Co_2C is formed with ease from Co^0 within 6 h of reaction and stably maintained with the help of Mn and Na. The catalyst demonstrates a high selectivity to lower olefins with superiorly low selectivity to both CO_2 and CH_4.

2. Experimental

2.1. Catalyst preparation

The composite oxide catalysts with different Co to Mn ratios were prepared by the "melting" method. During catalyst preparation, the anhydrous glucose, urea, and $Co(NO_3)_2{\cdot}6H_2O$ were mixed in a 250 mL beaker in a mass ratio of 3: 5: 2. The mixture was heated up to melt at 100℃ and stirred well for 0.5 h with a magnetic stirring device before adding the mixed solution that contained $Mn(NO_3)_2$ (in various amount for desired Co/Mn ratios for the catalysts) and 0.4 wt% Na_2CO_3 (based on the mass of the catalyst to be prepared). The same temperature and stirring speed were maintained for another 4.5 h before it was cooled to

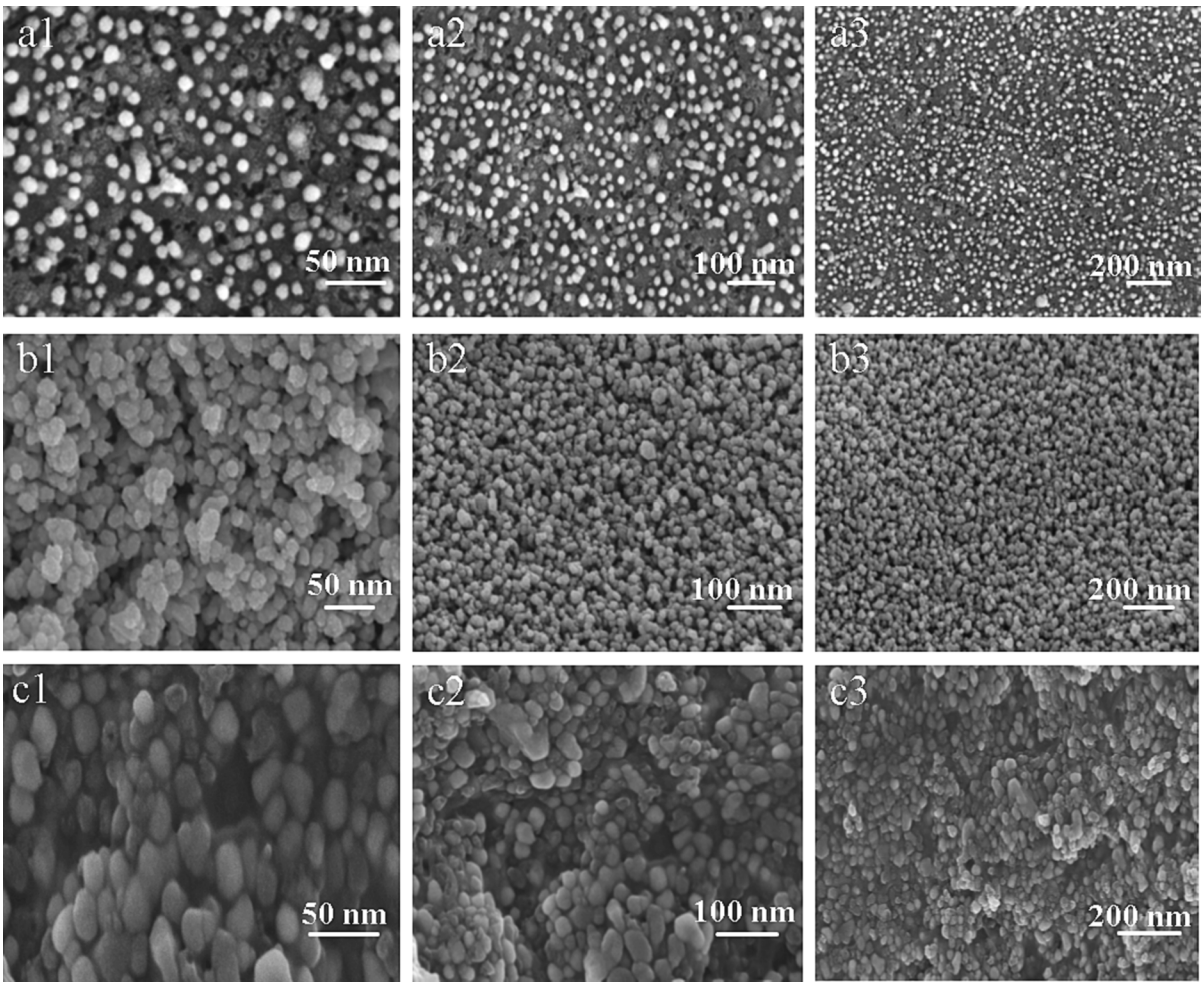

Fig. 1. SEM diagrams of the prepared catalyst at different stages with Co/Mn ratio at 2 (a: before carbon removal; b: pristine catalyst; c: spent catalyst).

room temperature. The paste-like mixture was then thermally treated in an oven at 180 ℃ for 24 h with N_2 protection to allow sufficient relaxation for the precursor. The foam-like catalyst precursor was then ground and calcined in a tube furnace under N_2 protection. The temperature ramped from room temperature to 400 ℃ with a rate of 2 ℃/min and was kept at the peak temperature for 3 h. The precursor was finally treated in a muffle furnace at 300 ℃ with static air for 3 h to remove carbon by oxidation. The remaining material was cooled to room temperature, and the cobalt-manganese composite oxide catalyst was prepared. The actual elemental content for Co and Mn was determined by ICP, and the results are given in Table S1 in the supporting information.

2.2. Characterization

To gain comprehensive details of the catalytic material and to correlate the performance of the catalyst with the microstructure, the pristine, reduced, and spent catalysts were characterized by XRD (X-Ray Diffraction), SEM (Scanning Electron Microscope), TEM (Transmission Electron Microscope), XPS (X-ray Photoelectron Spectroscopy), and ICP-OES (Inductively Coupled Plasma-Optical Emission Spectroscopy). The XRD analysis was conducted with a D8 Advance X-ray diffraction instrument from Bruker, operating at 40 kV and 40 mA with a scanning rate of 1°/min and a scanning angle (2θ) ranging from 20 to 80°. The identification of different phases was performed by comparing the pattern of signals with JCPDS standard files. The SEM analysis was carried out with a ZEISS Gemini SEM 300. The acceleration voltage was 3 kV, the resolution was 0.7 nm@15 kV, and the probe current was 3 PA-20nA. The TEM characterization was performed using a JEOL JEM-2100 instrument with an acceleration voltage of 200 kV. A sample for TEM was prepared by dispersing the catalyst in ethanol, followed by ultrasonication, and then loaded on a copper microgrid covered by a holey-carbon film. XPS analysis was performed by Thermo Scientific K-Alpha instrument equipped with a micro-focused monochromatic Al K α radiation (1486.6 eV). An appropriate amount of sample was prepared and placed in the sample chamber, and the pressure was decreased to be lower than 2.0×10^{-7} mbar. The spot size of radiation was adjusted to 400 μm, and the operating voltage was kept at 15 kV with a filament current of 6 mA. The exact Co and Mn contents in catalyst samples were analyzed by ICP-OES on Agient 700. The catalyst samples were pressed into pills and crushed to 280–450 μm particles. 0.05 g of the sample was then dissolved completely to form a pre-set volume of solution for the test.

2.3. Catalyst test

The FTO experiments with the prepared catalyst were carried out in a stainless-steel micro fixed-bed reactor (ID = 8 mm, L = 40 cm). The prepared cobalt-manganese composite catalyst was loaded into the constant temperature section of the fix-bed reactor with stainless steel balls to support the catalyst bed. The catalyst was reduced *in situ* by H_2 at atmospheric pressure at a flow rate of 2000 mL/h/g_{cat}. The temperature was increased from room temperature to 300 °C at a ramping rate of 2 °C/min and then kept at the peak temperature for 15 h. The reactor was then cooled down to 100 °C and purged by N_2 before introducing syngas. Subsequently, syngas with H_2/CO at the designed ratio was

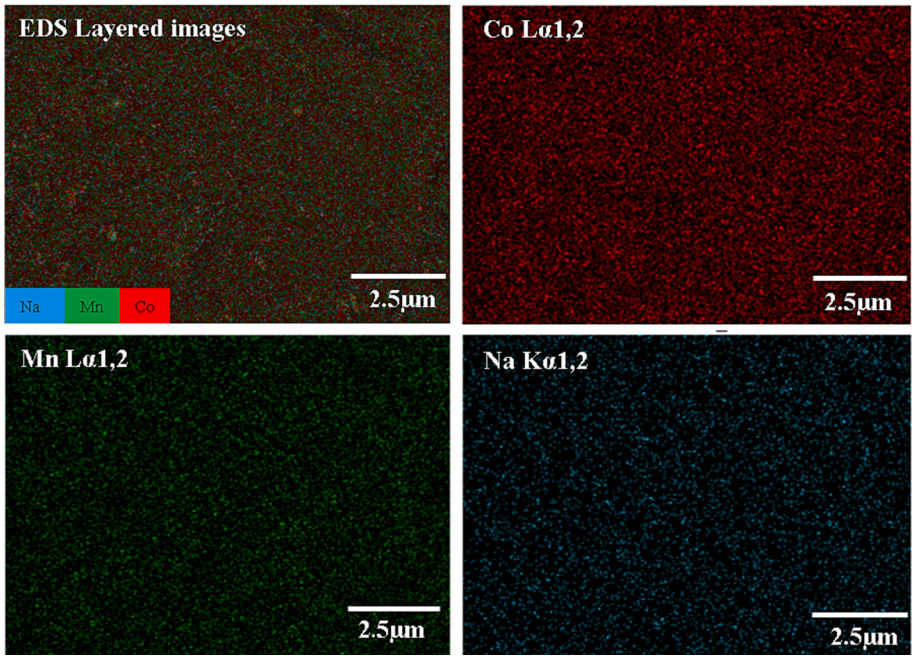

Fig. 2. The elemental mapping for the pristine catalyst with Co/Mn ratio at 2 (Co: in red color; Mn: in green color; Na: in blue color). (For interpretation of the references to color in this figure legend, the reader is referred to the web version of this article.)

introduced to the reactor for the FTO reaction. 10 % of nitrogen was included in the feed as the balance gas as well as the internal standard. To compare the product selectivity at a similar level of conversion among different catalysts, CO conversion was adjusted by changing the weight hourly space velocity (WHSV) from 2000 to 6000 mL/h/g_{cat} at 240 °C.

The conversation of CO (X_{CO}) was calculated using Eq. (1)

$$X_{CO} = 1 - \frac{CO\%_{out} \times MFR_{out}}{CO\%_{in} \times MFR_{in}} \quad (1)$$

where $CO\%_{out}$ and $CO\%_{in}$ represent the CO molar fractions in the outlet and inlet gases, respectively; MFR_{out} and MFR_{in} represent the molar flowrates of the outlet and inlet gases.

The CO reaction rate (r_{CO}, mol/h/g_{cat}) was calculated using Eq. (2)

$$r_{CO} = X_{CO} \times CO\%_{in} \times MFR_{in} \quad (2)$$

The selectivity to CO_2 (Sel_{CO_2}) was calculated using Eq. (3)

$$Sel_{CO_2} = \frac{CO_2\%_{out} \times MFR_{out}}{CO\%_{in} \times MFR_{in} \times X_{CO}} \quad (3)$$

where $CO_2\%_{out}$ represents the CO_2 molar fraction in the outlet gas.

The selectivity to C_nH_m ($Sel_{C_nH_m}$) (n is carbon number and m is the hydrogen number) was calculated using Eq. (4)

$$Sel_{C_nH_m} = \frac{n \times C_nH_m\%_{out} \times MFR_{out}}{r_{CO} \times (1 - Sel_{CO_2})} \quad (4)$$

where $C_nH_m\%_{out}$ represents the molar fraction of C_nH_m in the outlet gas.

The olefin to paraffin ratio (O/P) was calculated using Eq. (5)

$$O/P = \frac{C_nH_{2n}\%_{out}}{C_nH_{2n+2}\%_{out}} \quad (5)$$

where $C_nH_{2n}\%_{out}$ and $C_nH_{2n+2}\%_{out}$ represent the molar fraction of olefin and paraffin for specific carbon number n in the outlet gas.

After each run, the used catalyst was passivated before it was taken out for characterizations. During catalyst passivation, the reactor was purged with N_2 for 12 h at the same temperature of reaction and then cooled down to room temperature. A gas mixture with 1 % O_2 (N_2 as balance gas) was sent to the reactor to passivate the catalyst at atmospheric pressure for 4 h. After passivation, the catalyst was removed from the reactor and ultrasonically washed with carbon disulfide for 20 min. The sample, as the spent catalyst, was then washed with deionized water and dried at 60 ℃ before conducting further characterization.

To investigate the evolution of the catalyst during the transformation from the pristine to the active phases for the FTO reaction, the reaction behavior for the prepared catalyst was investigated during the initial period once it had been reduced by H_2 at the same condition. The time set for the reaction duration was 0.5, 1, 2, 4, and 6 h respectively, while 0 h means reduction only without feeding syngas to the reactor. When the catalyst had participated in the reaction for the set duration, the feed gas was switched from syngas to N_2 to follow the catalyst passivation procedure. It was hard to collect a complete set of data for short reaction periods in this dynamic experiment, we then mainly concentrated on the selectivity to olefins and paraffins by looking at the O/P ratios. The catalyst samples that have undergone different reaction durations were characterized by HRTEM and XRD for the dynamic evolution of the catalyst from the pristine state to its status when the reaction stabilized.

3. Results and discussion

3.1. The structural and morphological study

3.1.1. SEM analysis and elemental mapping for the catalyst

The pristine and used catalysts were analyzed by SEM for their microscopic morphology, and the result is presented in Fig. 1. The Co-Mn nanocomposite is formed after the catalyst precursor has been calcined in the tube furnace, as shown in Fig. 1a. The round-shaped nanocomposites are distributed evenly in a “pool” of graphite carbon. Fig. 1b shows the morphology of the prepared catalyst when graphite carbon has been removed by oxidation. It shows that the nanocomposite prepared by this method has a spherical morphology with uniform size and mono-dispersity. The morphology of the catalyst (Fig. 1c) has changed significantly after the FTO reaction, from the original spherical shape to an ellipsoidal shape with a smoother surface when compared to the pristine catalyst. The growth of the particles is in an oriented direction instead of a normally observed size increase for Co-based

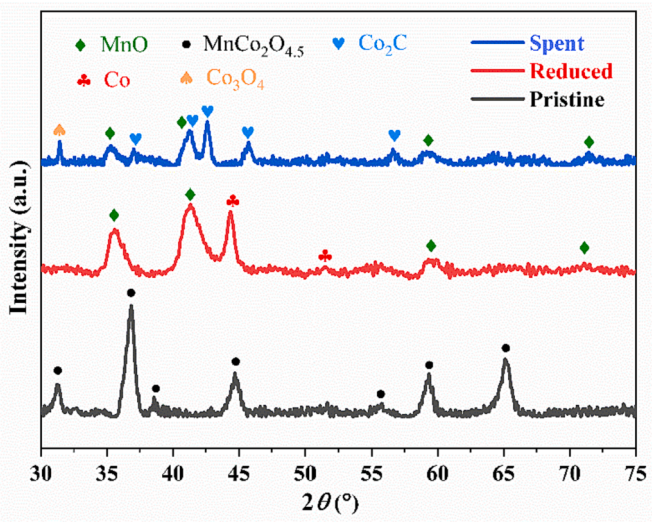

Fig. 3. XRD diagram for the pristine, the reduced, and the spent catalysts with Co/Mn ratio at 2.

catalysts in the FTS. It is highly likely that the adjacent round-shaped Co-Mn nano particles merged to form ellipsoidal-shaped Co_2C particles during carburization and reaction. The TEM results for the pristine and spent catalysts in Fig. 4, Section 3.1.3 will demonstrate the different shapes of the crystal facets of Co_2C. The dynamic evolution experiment later will also reveal the course of such merging. The elemental distribution in the nanocomposite for the prepared catalyst was characterized by EDX-mapping, and the result is shown in Fig. 2. The EDX-mapping exhibits the dispersion for each element as well as the overlayer for all elements of the catalyst, with Co in red, Mn in green, and Na in blue. The mapping result suggests that the catalyst prepared by this method has an excellent dispersion in all involved elements.

3.1.2. XRD analysis for the catalyst

The pristine, reduced, and spent catalysts with a Co/Mn ratio of 2 were analyzed by X-ray diffraction for their phase compositions, and the result is presented in Fig. 3. The pristine catalyst prepared in this work before activation (reduction) has high signal intensities at 31.26°, 36.82°, 44.83°, 55.77°, and 59.47°, and these are corresponding to the characteristic peaks of $MnCo_2O_{4.5}$ (JCPDS#32-0297). The prepared catalyst, therefore, possessed a single phase as $MnCo_2O_{4.5}$. Once it is reduced by H_2, the Co-Mn composite oxide transforms from $MnCo_2O_{4.5}$ to metallic Co (JCPDS#89-4307) and MnO (JCPDS#04-0326). No $MnCo_2O_{4.5}$ or any other Co-Mn composite or cobalt oxide(s) was observed for the reduced catalyst sample by XRD. According to the literature [24], Mn may hinder the reduction of Co^{2+} to Co^0, and the degree of reduction of Co^{2+} depends on the strength of the interaction between Co and Mn. We have observed similar phenomena, see Figure S1, when Na is not included in the prepared Co-Mn composite catalyst, also as $MnCo_2O_{4.5}$, can only be reduced to $Co_xMn_{1-x}O$ instead of Co^0. This suggests that Mn does hinder the reduction of Co. However, when Na is added during the preparation of the Co-Mn composite catalyst in this work, the reducibility of the catalyst changes completely as Co^0 instead of $Co_xMn_{1-x}O$ is derived for Co (Fig. 3). The result in Fig. 3 and S1 suggests that Na plays a crucial role in the successful reduction of Co and its liberation from the Co-Mn composite structure, either $MnCo_2O_{4.5}$ or $Co_xMn_{1-x}O$.

After the FTO reaction, the composition of the catalyst has transformed to Co_2C with the featured diffraction peaks appearing at 37.01°, 41.28°, 42.57°, and 45.75° (JCPDS#65-1457) [33], respectively, and MnO with the featured peaks at 36.36° and 43.72° (JCPDS#04-0326). The composition of the catalyst has changed from a single $MnCo_2O_{4.5}$ to Co_2C and MnO via Co^0 as the intermediate state. This confirms that Co_2C, instead of Co^0, is the active phase for the catalyst prepared in this work. The XRD result also suggests that the lattice planes of Co_2C formed under syngas are (210), (101), (020), and (111). The lattice plane information will be discussed in detail in the section of TEM characterization. The signal at 31.38°, which could be attributed to either $MnCo_2O_{4.5}$ or Co_3O_4 according to the database, appeared in the pristine and spent catalyst samples but not in the reduced one. As the peaks for $MnCo_2O_{4.5}$ has gone in the reduced sample, the reappeared peak at 31.38° is therefore attributed to Co_3O_4, which is a result of oxidation of Co^0 by H_2O formed by the FTO reaction. This will be addressed again later in Section 3.2.1 when the catalyst evolves during carburization. In addition, there is no diffraction signal identified for Na in all three samples, suggesting that Na is highly dispersed.

The XRD result here clearly demonstrates the phase change for Co during preparation, reduction, and carburization. Notably, Co^0 is presented in the reduced catalyst sample in this work, and it then transforms to Co_2C with the presence of syngas. In contrast, the Co-Mn composite catalysts prepared by other methods in the literature don't share the same transformation route for Co to derive Co_2C. The critical difference is that Co^0 is usually not observed in their reduced catalyst samples. For example, the catalyst prepared by the impregnation method may result in two separate oxides of Co_3O_4 and MnO [34], instead of Co-Mn composite. The co-precipitation method [35–39] yields a Co-Mn composite, and such composite cannot be reduced by H_2 to form metallic Co due to the strong interaction between Co and Mn, as suggested by the authors. It transforms from $MnCo_2O_{4.5}$ to $Co_xMn_{1-x}O$ and then to Co_2C directly with the presence of syngas.

However, the experimental evidence in this work supports us to hold a different opinion that Na is key to determining the successful reduction of Co-Mn composite to the metallic state Co. As a spinel structure, Co-Mn composite oxide, without transforming to independent Co and Mn species due to a strong interaction between Co and Mn (as shown by the XRD results in Figure S1) when Na is not added into the catalyst sample, works as a catalyst for the FTS/FTO as well, but with very high selectivity to CH_4 (as shown by the data in Table S2). When strong electron donor Na is added, the spinel structure of Co-Mn composite oxide could be reduced to Co^0 and MnO, but to different extents when different preparation methods are applied. The "melting method" here results in a much greater reduction extent, with mainly Co^0 in the reduced catalyst sample and consequently higher content of Co_2C after carburization (as the data shown in Figs. 3, 5, 7), all of which suggest that the interaction of Co-Mn in the spinel structure has been weakened. However, the precipitation method with the same elemental contents gives partially reduced Co-Mn composite, $Co_xMn_{1-x}O$ mainly after reduction, and a mixture of Co_2C and $Co_xMn_{1-x}O$ in the spent catalyst (Figure S7), suggesting that the strong interaction between Co and Mn in the spinel structure persist. With the evenly distributed Na (Fig. 2) in the catalyst due to the advantage of the catalyst preparation method in this work, the $MnCo_2O_{4.5}$, therefore, decomposes to separate Co^0 and MnO crystals successfully during H_2 reduction. The Co^0 with the presence of Na then transforms to Co_2C with ease when syngas is introduced to the reduced catalyst.

3.1.3. TEM analysis for the catalysts

The pristine and used catalysts were analyzed by TEM and HRTEM, and the result is given in Fig. 4. The prepared Co-Mn nanocomposite presents a uniform distribution in particles (Fig. 4a), and the average particle size is about 11 nm (Figure S2a), while the spent catalyst shows a much wider size distribution (Fig. 4c), and the average particle size has increased to about 21 nm (Figure S2b). The morphology shows that the crystal of the pristine catalyst is mainly spherical (Fig. 4b), and that of the spent catalyst (Fig. 4d) is diverse, with spherical, prismatic, and ellipsoidal shapes at wide dispersions. These changes match what we have seen in the SEM analysis section and confirm that adjacent nanoparticles have merged to form larger particles. The catalyst morphology has varied greatly when the FTS reaction takes place on the surface of

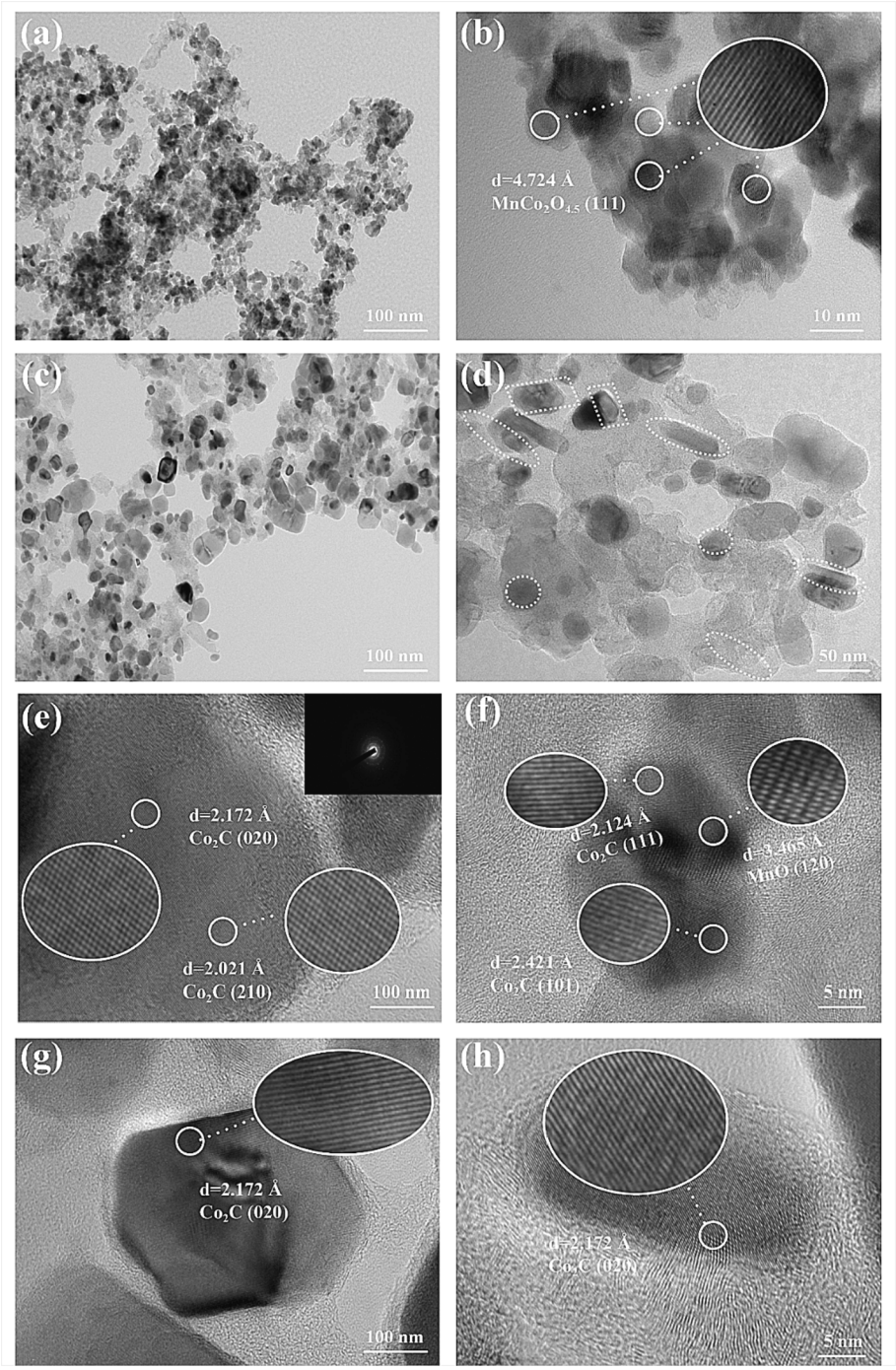

Fig. 4. TEM images for catalysts at different stages with Co/Mn ratio at 2 (a-b: pristine catalyst; c-d: spent catalyst) and different cobalt carbide crystal facets after reaction (e-h).

the catalyst, while the composition of the catalyst has also changed extensively. The phase attribution was verified by lattice stripe analysis. The lattice pitch of the pristine catalyst (Fig. 4b) is 4.72 \AA, corresponding to $MnCo_2O_{4.5}$ (1 1 1) facet. After reduction and reaction, the $MnCo_2O_{4.5}$ (1 1 1) has transformed to MnO (1 2 0) (Fig. 4f) with a lattice pitch of 3.46 \AA and Co_2C with at least four different crystal facets, including ellipsoidal Co_2C (2 1 0) with a lattice pitch of 1.98 \AA corresponding to the 45.75° characteristic peak of XRD spectrum, prismatic Co_2C (0 2 0) with a lattice spacing of 2.19 \AA corresponding to 41.27° characteristic peak of XRD spectrum, and round shaped Co_2C (1 1 1) and Co_2C (1 0 1) with pitches of 2.12 \AA and 2.42 \AA respectively. According to the literature [26], different crystalline facets exhibit different catalytic properties, with (1 0 1) and (0 2 0) facets capable of achieving high selectivity towards low-carbon olefins.

No Co^0 was found in the spent catalyst with the analysis results of XRD and TEM, although Co^0 is believed to be essential for the FTS reaction in the literature. Some early study [27] also suggests that Co_2C is unstable and could transform back to Co with the presence of H_2. The observed Co_2C with various facets stabilized as the active phases of the catalysts during the FTO reaction. Promoters such as Mn and Na are believed to help stabilize the Co_2C [40–43], which is confirmed in this work with no Co^0 but Co_2C only as the active phase in the catalyst. The transformation route of the Co-Mn composite in the prepared catalyst to Co_2C as the active phase has been discussed, while how the material

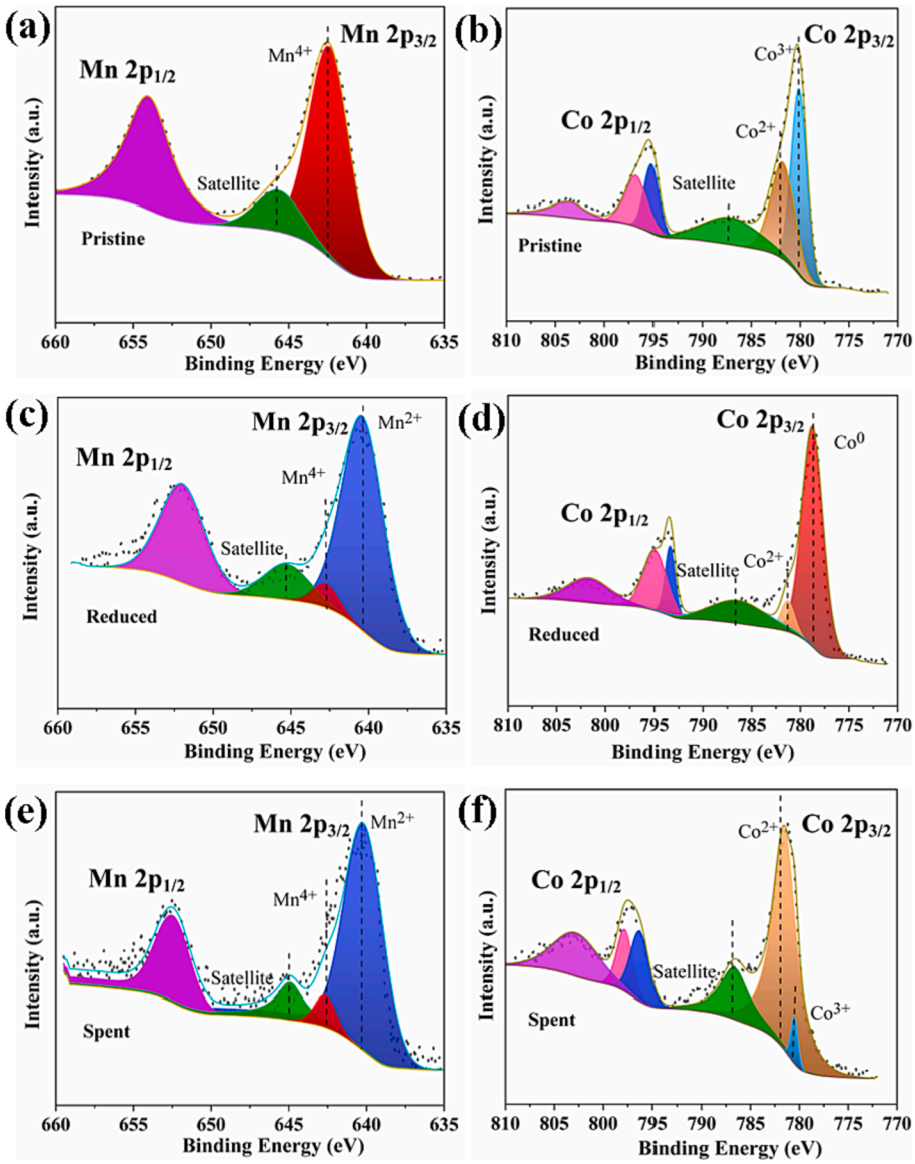

Fig. 5. Co 2p and Mn 2p XPS spectra of the catalysts with Co/Mn ratio at 2 (a and b pristine catalyst; c and d reduced catalyst; and e and f spent catalyst).

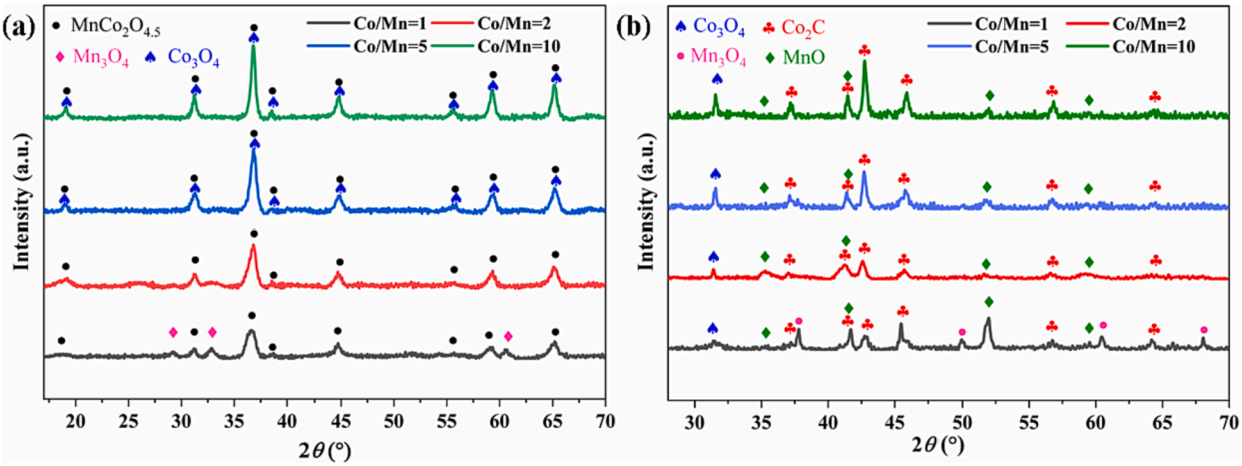

Fig. 6. XRD pattern of pristine and spent catalysts with different Co/Mn ratios (a: pristine catalysts; b: spent catalysts).

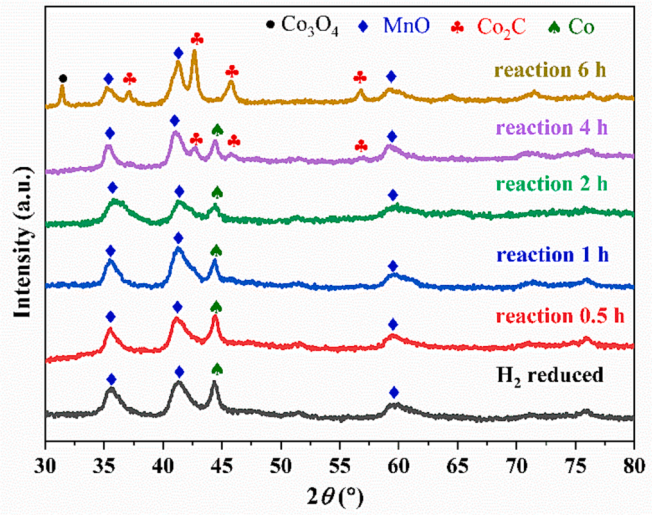

Fig. 7. XRD pattern for the Co-Mn catalyst with Co/Mn ratio at 2 (a: before and after reduction with H_2; b: during the initial 6 h of reaction).

evolved from the pristine catalyst to the active catalyst will be further studied later in Section 3.2.

3.1.4. XPS analysis for the catalyst

In addition to the morphological and phase characterizations above, the XPS was applied to analyze the valance states of elements in the pristine Co-Mn composite oxide, the reduced, and the spent catalysts. The XPS procedure in the Experimental was applied for the pristine and spent catalyst samples. The analysis for the reduced sample was done by reducing the sample *in situ* with H_2 at the same reduction temperature for 2 h prior to conducting the analysis, considering that the reduced Co-based catalyst is easily oxidized once it is exposed to the air. The full spectrum of XPS analysis for the pristine catalyst is given in Figure S3. The XPS result of Co 2p and Mn 2p for the catalyst at the three stages is shown in Fig. 5, and that of the C 1 s and O 1 s is given in Figure S4.

Both Co^{2+} (781.14 eV) and Co^{3+} (780.05 eV) are observed for the pristine catalyst in the Co 2p spectra (nCo^{3+} / nCo^{2+}=1.57), which correspond to the valance states of Co in the Co-Mn composite $MnCo_2O_{4.5}$. Once the catalyst is reduced, mainly Co^0 (778.41 eV) is found with a limited amount of Co^{2+}(nCo^0 / nCo^{2+}=11.61), suggesting that most of $MnCo_2O_{4.5}$ has been reduced to release metallic Co from the composite structure. This matches the XRD result for the reduced catalyst, see Fig. 3. It is also noticed that no Co oxides peaks were identified in the reduced sample in the XRD result but not all Co is identified as Co^0 valance state by XPS. It may be due to some small crystals that are hard to reduce, which is often experienced for the Co-based catalysts for the FTS [44]. The small crystals may not be identified by the XRD to form featured diffraction peaks but can be picked up by the XPS. Other than this, an incomplete reduction may also happen as a shorter reduction period (2 h for the analysis versus 15 h in the experiment) was applied during the *in situ* study of XPS. Nevertheless, the reduction of the Co^{2+} and Co^{3+} in the $MnCo_2O_{4.5}$ to Co^0 was achieved. After carburization during the reaction, Co^{2+} becomes a predominant state with a limited amount of Co^{3+} (nCo^{2+} / nCo^{3+}=21.13). Combing the result provided by XRD and HRTEM, most of Co is now in the form of Co_2C [45,46] as neither CoO nor $Co_xMn_{1-x}O$ is identified. This could also be supported by the carbide peak found in the C 1 s spectra (Figure S4). The evolution of Co valance states in the pristine, reduced, and spent samples revealed by the Co 2p spectra agree with the XRD and HRTEM analysis results by giving us two important facts that Co can be reduced from the $MnCo_2O_{4.5}$ to Co^0 and most of Co is in the form of Co_2C during the reaction.

Regarding the Mn 2p diagram, Mn is found to be Mn^{4+} for the pristine catalyst as the peak appears at 642.48 eV in the spectrum, which corresponds to the XRD and HRTEM results for the pristine catalyst sample as Mn has combined with Co and O to form $MnCo_2O_{4.5}$ [47]. While in the reduced sample, majority of Mn shows in the valance state of Mn^{2+} as the peak shifts to 640.25 eV, with a small amount in Mn^{4+} (nMn^{2+}/ nMn^{4+} =16.82), suggesting that Mn element is in the form of MnO [48]. The change of valance state of Mn here is actually strong evidence to support that the Co has been successfully liberated from Co-Mn composite during catalyst reduction as the phase separation of $MnCo_2O_{4.5}$ forms two separate crystals, MnO and Co^0. In the spent catalyst sample, the content of Mn^{4+} (nMn^{2+}/ nMn^{4+} =15.35) is close to that in the reduced sample, suggesting that Mn^{2+} is stably maintained during the carburization process and reaction.

Lattice O was the dominant signal in O 1 s spectrum for the pristine catalyst (Figure S4), which is expected because Co-Mn composite oxide was identified as the dominant species in the precursor catalyst. Once the catalyst is reduced, the lattice O has dropped to a very low fraction, suggesting the large fraction of lattice O has been taken out during the reduction. The proportion of lattice O becomes even smaller in the spent catalyst sample, which may be a result of the amplified OH peak caused by the products.

3.1.5. Mn effect on the active phase of the catalyst

To investigate the effect of Mn additives on the catalyst regarding Co-Mn composite structure and catalytic performance, we prepared catalysts with different Mn content and marked them as Co/Mn ratios with values of 1, 2, 5, and 10. The elemental analysis for these catalysts is given in Table S1. Its structural effect is discussed here with the XRD analysis, and the effect of Mn on product selectivity will be discussed in Section 3.3.1.

Fig. 6 shows the XRD diagram of the catalysts prepared with different Co/Mn ratios. According to the database (JCPDS#43-1003 and JCPDS#32-0297), the diffraction peaks for Co_3O_4 and $MnCo_2O_{4.5}$ appear at almost the same 2θ location. For the pristine catalysts (Fig. 6a), the signals get intensified when the Co/Mn ratio increases, which is caused by a higher content of Co_3O_4 in the samples. While the XRD pattern for the sample with a low Co/Mn ratio (Co/Mn = 1), Mn_3O_4 peaks are identified at 50.98°, 60.02°, and 67.86° (JCPDS#18-0803). XRD patterns for both Co_3O_4 and Mn_3O_4 with the same catalyst preparation method used in this work are given in Figure S5 as a reference. The XRD pattern of the spent catalyst (Fig. 6b) shows diffraction peaks corresponding to Co_2C, MnO, and Co_3O_4. For all spent catalysts, Co_2C with the four facets mentioned above with the characteristic peaks at 37.01°, 41.28°, 42.57°, and 45.75° are all observed, revealing that $MnCo_2O_{4.5}$ has been carburized into these cobalt carbides at the investigated Co/Mn ratios with the presence of syngas during the reaction. Co_3O_4 (31.38°) is detected in the spent catalysts for all four Co/Mn ratios, and a higher ratio gives a stronger Co_3O_4 intensity as more Co has been oxidized during the reaction due to higher availability of Co^0.

3.2. The dynamic evolution of the catalyst

The compositions, structure, and morphology of the pristine and spent catalysts have been clearly shown with the results above. To further understand the evolution of the catalyst from the just prepared state to the active status and the corresponding performance during the dynamic evolution, we ran FTO experiments at the same conditions with different periods during the initial stage when the catalyst had been reduced with H_2, as has been introduced in the Experimental section. The SEM, XRD, and HRTEM results for the catalysts that have undergone different reaction durations are reported here and the reaction data during catalyst evolution will be discussed in Section 3.3 [5].

3.2.1. SEM analysis during dynamic evolution of the catalyst

Figure S6 presents the morphology of the catalyst by SEM at different reaction durations. The freshly reduced catalyst shows a spherical shape,

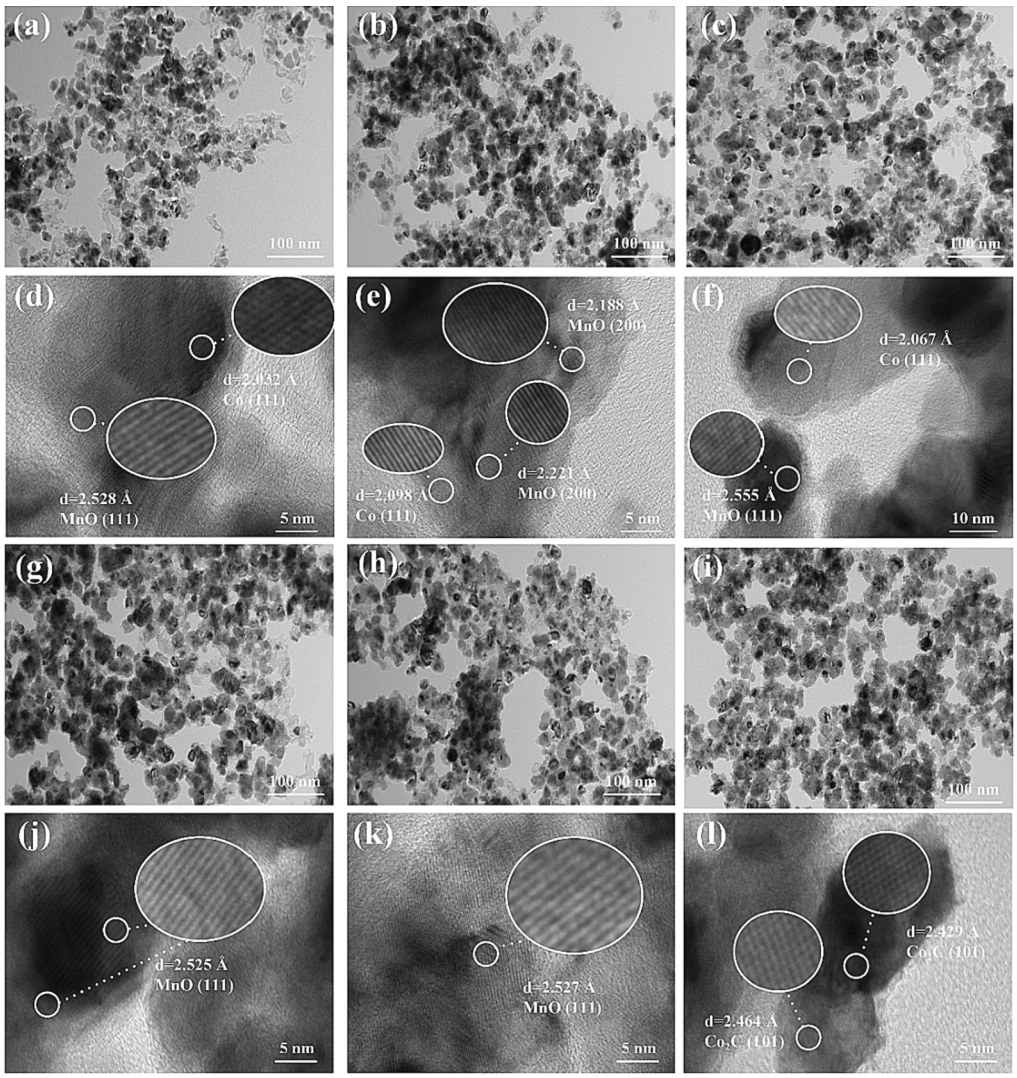

Fig. 8. TEM images of the catalyst at different reaction stages with Co/Mn ratio at 2 (a-b: after 15 h of H_2 reduction, c-d: after 0.5 h of reaction, e-f: after 1 h of reaction, g-h: after 2 h of reaction, i-j: after 4 h of reaction, k-l: after 6 h of reaction.).

and the metal nanoparticles were partially clustered. Once syngas is introduced and the carburization process initiates, the catalyst morphology starts to change slowly, and particle size becomes larger gradually. More ellipsoidal-shaped particles are eyed when the reaction duration extends. With such unceasing change, the nanoparticles eventually reached a morphology shown in Fig. 1c.

3.2.2. XRD analysis during dynamic evolution of the catalyst

Fig. 7 illustrates the XRD patterns for the catalyst with H_2-reduced and during the reaction. The XRD result here suggests that the metallic Co can be transformed to Co_2C mainly within 6 h under the syngas atmosphere at 0.1 MPa(g). The appearance of Co_2C starts from 4 h of reaction, and by the end of 6 h, the marked Co_2C with all four different facets can be identified on the XRD spectrum with signals in good intensity. Meanwhile, the Co^0 peak (44.23°) starts to shrink when Co_2C appears, and it vanishes at the end of 6 h. We also notice that Co_3O_4 (31.38° at XRD spectrum of 6 h) has no intensity when the catalyst is freshly reduced and appears at the end of 6 h, suggesting that part of Co^0 is oxidized by H_2O in the reactor. The result here confirms that the peak at 31.38° that we noticed in Fig. 1 should be attributed to Co_3O_4 instead of $MnCo_2O_{4.5}$. Co_3O_4 is believed to have the water–gas-shift (WGS) activity, so CO_2 will be formed by this catalyst [49].

3.2.3. TEM analysis during dynamic evolution of the catalyst

The TEM analysis for the catalysts that have undergone different reaction durations is presented in Fig. 8. The freshly reduced catalyst has lattice pitches of 2.03 Å and 2.53 Å, corresponding to the Co (1 1 1) and MnO (1 1 1). These match the peaks at 44.23° and 35.24° of the XRD spectrum in Fig. 8. During reduction, the reduced Co migrates out of $MnCo_2O_{4.5}$ and separates from MnO. The formed Co^0 and MnO are scattered next to each other. Clearly, with reduction by H_2, the prepared Co-Mn composite oxides have separated into Co^0 and MnO. When the reaction duration extends, the Co lattice becomes less identified. Until 6 h of reaction, the prismatic Co_2C (1 0 1) starts to appear.

Both the dynamic XRD and HRTEM results suggest that the Co-Mn composite could be reduced to two separate phases, Co^0 and MnO, and the transformation of Co^0 to Co_2C can be achieved within 6 h with the presence of syngas at 240 ℃. The period needed for the transformation of Co^0 to Co_2C is much shorter when compared to some previous work when the catalyst was prepared by co-precipitation and impregnation methods [31].

3.3. FTO performance of the catalysts

We performed a series of experiments to investigate the performance of the catalysts prepared by the “melting” method. The catalytic

Table 1
Catalytic performance with different Co/Mn ratios when $H_2/CO = 2$ in the feed.

Entry	Catalyst	Pressure (MPa)	CO conv.(C%)	$C_{2-4}^{=}$ sel.(C%)	$C_{5-8}^{=}$ sel.(C%)	CH_4 sel.(C%)	O/P ratio						
							C_2	C_3	C_4	C_5	C_6	C_7	C_8
1	Co/Mn = 1	0.1	12.48	49.88	25.38	10.04	9.64	10.45	10.56	7.60	6.14	4.37	3.78
2		1	12.70	46.95	17.83	14.59	2.16	4.79	5.12	4.44	3.22	2.66	2.28
3		2	13.96	34.84	10.54	16.18	1.31	1.84	1.94	1.37	1.46	1.62	1.48
4	Co/Mn = 2	0.1	10.75	52.72	21.06	11.46	7.57	11.68	11.85	7.90	5.22	3.67	2.61
5		1	11.25	44.17	15.72	17.27	4.09	5.20	4.79	3.09	2.84	2.48	1.29
6		2	14.42	35.77	14.45	21.77	1.63	3.27	2.86	1.84	1.68	1.65	1.06
7	Co/Mn = 5	0.1	12.11	52.13	20.13	12.82	8.33	10.88	11.76	7.19	5.39	2.89	1.12
8		1	14.74	44.97	16.81	20.23	3.65	5.13	5.08	3.39	3.27	3.15	3.01
9		2	17.30	26.92	4.50	31.99	0.57	1.45	1.62	1.20	1.37	1.60	1.57
10	Co/Mn = 10	0.1	6.83	56.57	16.49	13.74	7.86	9.67	9.02	4.46	2.87	3.19	2.47
11		1	10.84	40.59	11.63	24.83	1.55	3.41	3.68	2.54	2.32	2.21	2.36
12		2	13.52	26.15	5.01	31.04	0.59	1.42	1.68	1.37	1.32	1.12	0.92

Reaction conditions: T = 240 ℃, $H_2/CO = 2$, WHSV = 3000 mL/(h·g_{cat}) (Selectivity of olefins is based on the formed HCs, while the CH_4 selectivity is based on the converted CO).

Table 2
Catalytic performance with different Co/Mn ratios when $H_2/CO = 1$ in the feed.

Entry	Catalyst	Pressure (MP))	CO conv.(C %)	$C_{2-4}^{=}$ sel.(C%)	$C_{5-8}^{=}$ sel.(C%)	CH_4 sel.(C %)	O/P ratio						
							C_2	C_3	C_4	C_5	C_6	C_7	C_8
1	Co/Mn = 1	0.1	8.80	45.43	31.25	4.49	12.69	13.98	15.01	9.47	9.68	8.14	7.64
2		1	8.86	40.5	24.81	11.77	3.35	5.03	5.68	4.06	3.80	3.55	3.53
3		2	12.77	32.73	18.36	16.59	1.35	2.40	2.66	1.72	1.70	1.60	1.42
4	Co/Mn = 2	0.1	7.72	60.26	22.7	4.95	31.78	15.67	12.98	7.73	6.91	5.63	2.44
5		1	8.13	53.94	14.48	11.37	19.41	5.44	4.14	5.11	4.39	4.07	3.59
6		2	11.91	46.43	13.23	19.45	2.84	4.61	4.46	3.03	3.07	2.58	2.42
7	Co/Mn = 5	0.1	6.83	54.98	23.73	7.77	11.62	13.49	14.68	9.35	8.13	2.83	0.83
8		1	12.67	45.41	22.84	10.24	4.76	5.60	5.32	3.57	4.32	2.67	1.89
9		2	13.10	32.79	13.27	21.00	0.97	1.91	2.22	1.50	1.79	1.33	1.27
10	Co/Mn = 10	0.1	3.40	50.06	28.86	5.87	14.04	11.39	11.13	8.05	7.46	5.76	5.03
11		1	7.63	41.02	21.28	16.68	4.52	3.79	4.73	3.92	3.0.81	3.09	2.57
12		2	11.42	34.45	11.82	21.78	0.93	1.79	2.40	1.89	1.83	1.78	1.56

Reaction conditions: T = 240 ℃, $H_2/CO = 1$, WHSV = 6000 mL/(h·g_{cat}) (Selectivity of olefins is based on the formed HCs, while the CH_4 selectivity is based on the converted CO).

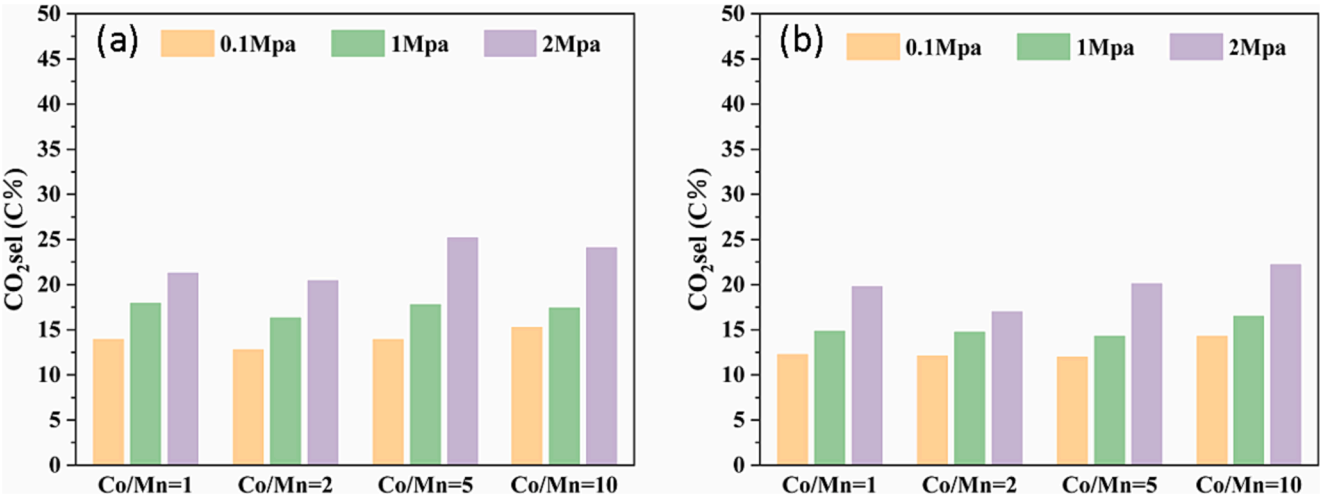

Fig. 9. CO_2 selectivity under the investigated conditions (a: T = 240 ℃, $H_2/CO = 2$, b: T = 240 ℃, $H_2/CO = 1$).

performance, including selectivity to olefins, CH_4, and CO_2 under different pressures and H_2/CO ratios is studied, and the correlation between the performance and the catalyst properties is discussed. The effect of Mn content on the reaction performance of Co_2C-based catalysts is evaluated [50]. The selectivity of olefins during the carburization of Co^0 was also recorded and discussed. And finally, we evaluated the stability of the catalyst by running the experiment for 100 h. The performance of the prepared Co-Mn composite as the precursor catalyst to form Co_2C for the FTO is summarized in Tables 1 and 2 with Co/Mn ratio, reaction pressure, and H_2/CO ratio in the feed gas. The CO_2 selectivity under various conditions with different Co/Mn ratios is plotted in Fig. 9.

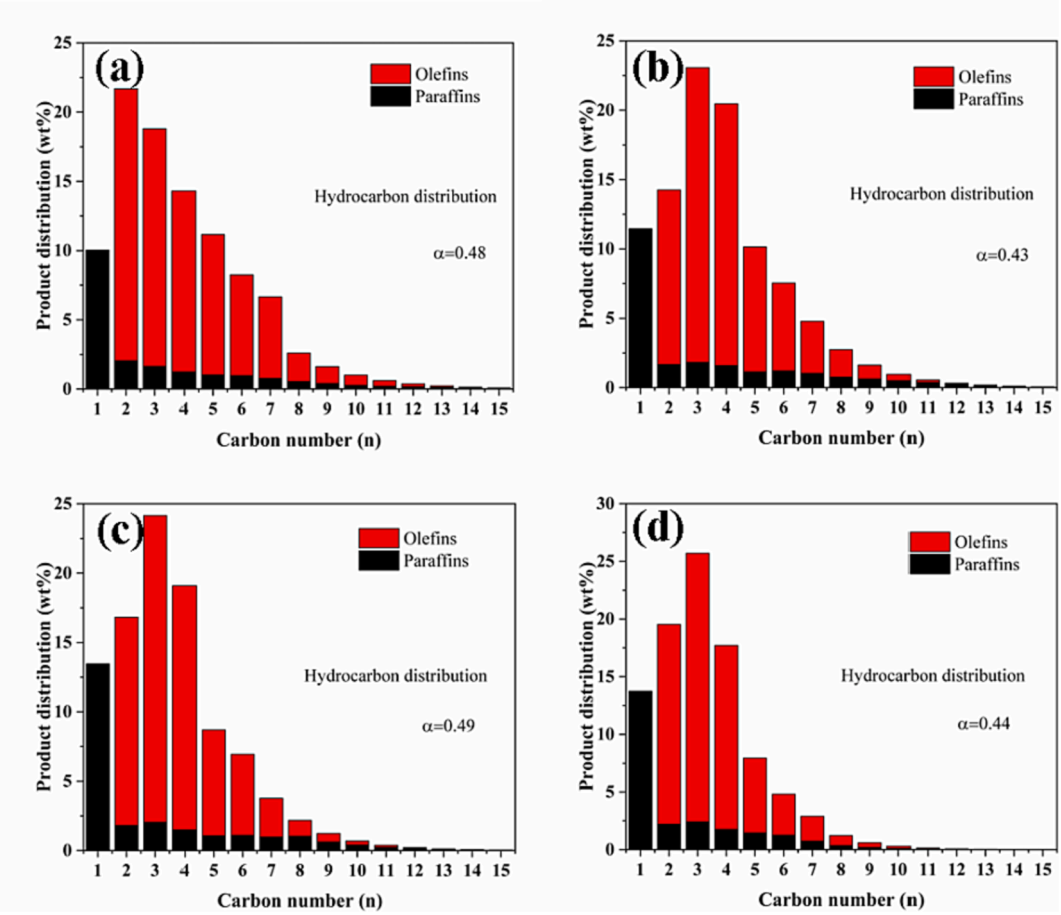

Fig. 10. Product distribution for catalysts with different Co/Mn ratios (a,1; b, 2; c, 5; d, 10) with $H_2/CO = 2$ in the feed gas (T = 240 ℃, P = 0.1 MPa(g), WHSV = 3000 mL/(h·g_{cat}).

3.3.1. Olefin selectivity with the prepared catalyst

Data in Tables 1 and 2 show that the derived Co_2C catalysts demonstrate high selectivity to lower α-olefins. Similar to the data reported for Co_2C in the literature, a low operation pressure favors the selectivity to olefins. When 0.1 MPa(g) pressure was set for the reactor, the selectivity to C_2-C_4 olefins could be as high as more than 60.26 % with high olefin/paraffin ratios, such as 31.78 for C_2, 15.67 for C_3 and 12.98 for C_4. When the operating pressure is increased to 2 MPa(g), the corresponding olefin/paraffin ratios drop rapidly to 2.84, 4.61, and 4.46, respectively. Olefin to paraffin ratios decreases with the increase in carbons numbers. This behavior has been observed widely in the studies of the FTS as the hydrogenation capability increases when the carbon number gets larger. The catalyst gives a low selectivity to CH_4 at low operating pressure, corresponding to the high selectivity to olefins. This suggests that the hydrogenation ability of this catalyst (especially with (1 0 1) and (0 2 0) facets suggested by the literature), either to the $–CH_2–$ monomer or to the olefins absorbed on the catalyst surface, is extremely weak. Co_2C favors the desorption of the unsaturated HCs once they are formed on the active sites [51]. Such weak adsorption reduces the probability of the short-chain HCs undergoing a further chain growth reaction, therefore resulting in low α values for the products (Figs. 10 and 11). Crystal size has been reported to affect the products as well. When Co_2C nanoparticles are larger than 7 nm, both intrinsic activity and product selectivity don't depend on the particle size [50]. In this work, the particle sizes of Co_2C are in the range of ~20 nm (Section 3.1.3 and Figure S2), implying that the size effect is not significant to the performance of the catalysts. An increase in operating pressure and the H_2/CO ratio prompts H_2 partial pressure in the reactor, favoring hydrogenation of the olefins. The CH_4 selectivity could increase from below 5 % to more than 30 % when H_2 partial pressure and Mn content both favor the CH_4 formation on the same Co_2C active sites.

We also include the selectivity to C_5-C_8 olefins in the reported data as we believe that the value of FTO resides both on lower olefins and higher olefins. The rich olefins with higher carbon numbers produced by the FTO process are value-added chemical feedstocks that other syngas conversion technologies, such as MTO and OX-ZEO, could not provide. When the reaction pressure is low, and the H_2/CO at 1, the O/P ratio for C_8 is still as high as 3.58 with Co/Mn ratio at 2 in the catalyst, meaning more than 78 % of C_8 is in olefin. High olefin selectivity for C_2-C_8 provided by this catalyst offers good opportunities for further conversion of the rich olefins to high value-added oxygenates, which will significantly improve the profit for the overall process.

The data in the tables also show that the change of operating pressure has a limited effect on the reaction rate for the Co_2C catalyst, suggesting that the rate-limiting step does not reside on the adsorption of the reactants but rather on the activation of CO and H_2. Unlike Co, Co_2C demonstrates a weak ability to dissociate H_2 [52] as H_2 is usually the limiting factor for the reaction rate in the FTS. A lower hydrogen dissociating rate also inhibits the formation of saturated HCs.

3.3.2. Product distribution

As a lower pressure favors the selectivity to the olefins, we, therefore, plotted the product distribution for the catalysts with different Co/Mn ratios at two feed gas ratios at 0.1 MPa(g) operating pressure. The chain-growth probabilities for these product distributions are calculated. The α values are low for the prepared catalysts with different Co/Mn ratios at the testing conditions. This features the catalyst suitability for the production of short-chain olefins. It is noticed that at some conditions, for

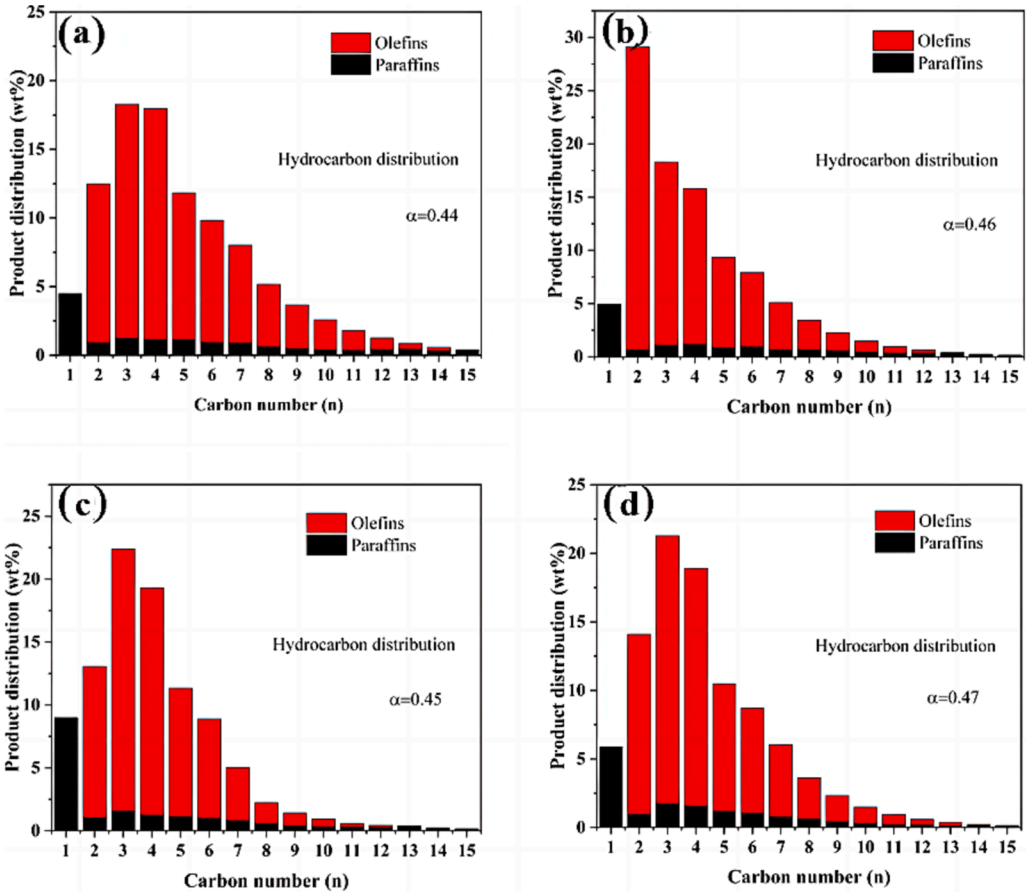

Fig. 11. Product distribution for catalysts with different Co/Mn ratios (a,1; b, 2; c, 5; d, 10) with $H_2/CO = 1$ in the feed gas (T = 240 ℃, P = 0.1 MPa(g), WHSV = 3000 mL/(h·g_{cat}).

example, in Fig. 10a and 11b, C2 presents a higher selectivity than C_3 while at the majority of conditions, C_3 shows the highest selectivity. This offers a possibility of adjusting the Co/Mn ratio and the operating conditions to achieve a further tunable selectivity of C_2 olefin to other olefins.

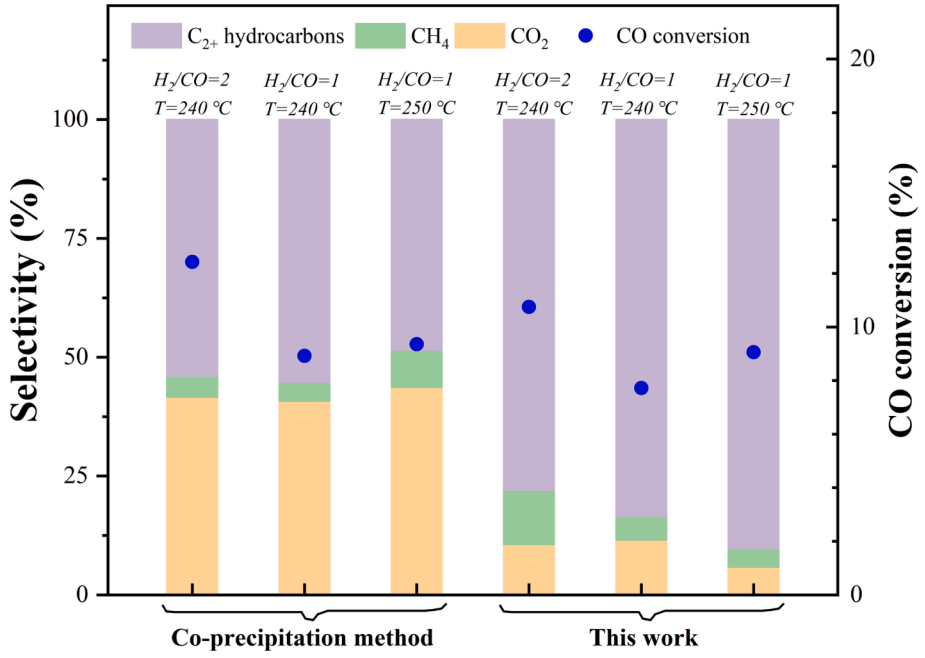

Fig. 12. Selectivity to CO_2, CH_4, and HCs under the same conditions for the catalysts prepared by the melting method and co-precipitation method with the same elemental contents (Co/Mn ratio at 2, 0.4 wt% Na).

3.3.3. Effect of Mn on the product selectivity

During the transformation of the Co-Mn composite to Co_2C, Mn is released from the Co-Mn composite oxide ($MnCo_2O_{4.5}$) to form MnO. MnO and Na are critical for stabilizing Co_2C in his work, and donating electrons to Co_2C also plays a vital role in product selectivity. As an electronic and structural promoter, Mn has a regulatory effect on the morphology of Co_2C nanoparticles and facilitates the formation of specific facets (0 2 0) and (2 1 0) [24]. Our data shows that a higher selectivity to olefins can be achieved in general, especially for the higher carbon numbers when Mn content is high. The catalyst demonstrated higher O/P ratios for C_5-C_8 olefins with Co/Mn ratio at 1 when other conditions are the same. A higher Mn content favored the desorption of unsaturated olefinic products before they convert to saturated paraffins, creating chances for the unsaturated olefins to reabsorb on the active sites for further chain growth reaction with the adjacent $–CH_2–$ monomers that are favored by Mn as well. Therefore, the chain growth reaction increases the formation of longer chain HCs and decreases the selectivity to lower α-olefins. A lower Mn content in the catalyst favors the formation of CH_4, which is undesired in the FTS and FTO as a high CH_4 selectivity reduces the carbon efficiency. A lower Mn content reduces the desorption of $–CH_2–$ monomers from the active sites and prompts the hydrogenation of the monomers to form CH_4. Meanwhile, there is no straightforward correlation between the Mn content and the CO_2 selectivity, as shown in Fig. 9, as a matter of fact that WGS for CO_2 formation is a result of both the property of the catalyst and the partial pressure of H_2O in the reactor.

The data obtained also suggest that Co and Mn should be in reasonable proportion to balance the performance of the catalyst. When Mn content is too low, the binding between Co and Mn is reduced. Therefore, it may reduce the formation of specific facets of cobalt carbide and affect the selectivity to olefins. When Mn content is too high, it may cover the surface of Co and inhibits the exposure of Co_2C, consequently reducing the catalytic performance. With the increase of the Co/Mn ratio, as shown in Tables 1 and 2, the O/P ratio for lower carbon numbers first increased and then decreased. When the Co/Mn ratio was at 2, we can obtain 60.26 % selectivity to C_2-C_4 olefins with an O/P ratio in a range of 31.78–12.98 based on the overall HCs produced, 22.70 % selectivity to C_5-C_8 olefins with O/P ratio in a range of 7.73–2.44. In comparison, the selectivity to CO_2 and CH_4 is 11.49 % and 4.95 %, respectively, with H_2/CO ratio at 1 in the feed gas. Therefore, Co/Mn = 2 can be regarded as the optimal ratio in terms of the performance of the catalysts in this work.

3.3.4. CO_2 selectivity of the catalysts

The catalyst prepared in this work gives a low CO_2 selectivity with Co_2C as the active sites and high selectivity to olefins both for C_2-C_4 and C_5-C_8. Fig. 9 summarizes the CO_2 selectivity at two gas ratios and three pressures adopted for the catalysts with different Co/Mn ratios. Generally speaking, the Co_2C transformed from $MnCo_2O_{4.5}$ via Co^0 demonstrates a low CO_2 selectivity. It is below 20 % for most of the conditions except when the catalyst was tested at 2 MPa(g) pressure, which is usually not adopted when lower olefins are the preferred products with Co-based catalysts. A low H_2/CO ratio and a low reaction pressure benefit the low selectivity to CO_2, which agrees with the experimental result in the literature [53]. We further compared the activity (as shown by CO conversion) and selectivity of CO_2 and CH_4, for the Co_2C catalysts prepared by the melting method in this work and the precipitation method adopted from the literature [26] with the same elemental contents (Co/Mn ratio at 2 and 0.4 wt% Na), and the results are presented in Fig. 12 below. Under close CO conversions at 240 and 250 ℃, the catalyst prepared by the method in this work demonstrates much lower CO_2 selectivity but similar CH_4 selectivity. Similar to the data reported in the literature when the precipitation method is used, the catalyst gives more than 45 % C_1 (CO_2 + CH_4) selectivity. With high selectivity to the olefins, C_{2+} products produced here could be regarded as high-value products. Therefore, the catalyst prepared by the method in this work demonstrates superior carbon efficiency.

When selectivity to lower olefins is highly emphasized, drawbacks for the overall carbon efficiency, such as high CO_2 and CH_4 selectivity, are often observed, depending on the category of the catalysts. With Co_2C catalysts derived from Co-Mn composite, we usually experience more than 40 % of CO_2 selectivity [54]. Generally speaking, CO_2 selectivity in the FTS and FTO reaction system is decided by both the catalytic material and the concentration of H_2O vapor that the active sites face [55]. With the characterization results, we can see that similar facets for Co_2C are derived in this work compared to works in the literature. It is believed that the product selectivity is decisive by the active sites of the catalytic material, which is fair, while the result in this work suggests that the composition in the Co_2C catalyst as well as the transformation pathway from the precursor catalyst to the final active Co_2C sites are crucial factors that decide the CO_2 selectivity.

The characterization of the catalyst in this work confirms that it contains mainly Co_2C and a limited amount of Co_3O_4 (11.24 % as calculated by the XRD result in Fig. 3). Co_3O_4 is active for WGS [49], so an even lower CO_2 selectivity should be expected if the catalyst contains Co_2C only. This implies that high CO_2 selectivity on Co_2C catalysts in the literature should not be attributed to Co_2C only but also to the presence of other materials, such as the untransformed Co-Mn oxides from the precursor catalyst. Recent work with DFT calculation agrees with the speculation here that Co_2C by itself does not hold WGS activity under FTS/FTO conditions [55]. As a matter of fact, the catalysts prepared in this work share the same or similar elemental compositions as those in the literature when high CO_2 selectivity is experienced [56]. It is, therefore, inappropriate to attribute the large difference in CO_2 selectivity to the elemental content or promoters. However, the different catalyst preparation methods here and in the literature do result in different active phases during the FTO reaction. The difference in CO_2 selectivity relies on the composition of catalysts under reaction, with Co_2C identified as the active phase in this work without $Co_xMn_{1-x}O$, but the co-existence of Co_2C and $Co_xMn_{1-x}O$ in some other works [26,30]. The XRD results for the catalyst prepared by the co-precipitation method [26] at pristine, reduced, and spent status are presented in Figure S7. With the same reduction procedure stated in the Experimental part, only a fractional Co was successfully liberated from the composite structure. After conducting the FTO reaction, $Co_xMn_{1-x}O$ and Co_2C are observed to co-exist in the catalyst sample. This is the intrinsic difference from the feature that no $Co_xMn_{1-x}O$ is identified in the spent catalyst sample prepared by the melting method. The reaction data for the catalyst prepared by the precipitation method show that more than 40 % CO_2 was obtained when only fractional Co has transferred to Co_2C but still a large fraction remained in the $Co_xMn_{1-x}O$ composite structure. We, therefore, believe that the presence of $Co_xMn_{1-x}O$ is the decisive cause of a higher CO_2 selectivity than Co_2C itself that has been observed in the FTO in the literature.

The characterizations of the catalyst samples at different stages provide a clear clue why $Co_xMn_{1-x}O$ co-exists by the co-precipitation method in the literature but not by the method reported in this work. As has been discussed in Section 3.1.2, Na plays a crucial role in the successful reduction of Co from $MnCo_2O_{4.5}$, i.e., to Co^0 when Na is available to the Co-Mn composite, and to $Co_xMn_{1-x}O$ when no Na is available for the composite. The elemental mapping reported in the literature by co-precipitation shows uneven dispersion of Na in the catalysts [41]. Therefore, not all the formed $MnCo_2O_{4.5}$ after calcination can be reduced to Co^0 successfully, and a lengthy carburization process is usually required for a slow, but yet not complete, the transformation of $Co_xMn_{1-x}O$ to Co_2C in some previous works [26]. As with a very even Na dispersion (Fig. 2), the $MnCo_2O_{4.5}$ prepared in this work could be reduced to form Co^0 and then carburize to Co_2C with ease. Therefore, we conclude that the low CO_2, as low WGSR activity of the catalyst in this work, is a result of higher content of Co_2C in the catalyst and without $Co_xMn_{1-x}O$, which is responsible for the WGSR. The well dispersion of Na is the key factor that ensures the high Co_2C content by facilitating the

Table 3
Olefin/paraffin ratios for C_2-C_5 during the course of transformation of Co^0 to Co_2C.

Reaction time	C_2 O/P	C_3 O/P	C_4 O/P	C_5 O/P
0.5 h	5.10	10.46	12.74	8.18
1 h	8.63	16.54	16.30	12.31
2 h	6.28	13.68	14.37	9.23
4 h	7.46	14.86	16.00	11.35
6 h	6.40	8.44	9.00	7.45

Reaction conditions: T = 240 ℃, H_2/CO = 2, WHSV = 2000 mL/(h·g_{cat}), Co/Mn = 2.

easy reduction of Co from $MnCo_2O_{4.5}$ to Co^0 (Fig. 3, 5 and S8) and then the formation of Co_2C from Co^0during carburization.

3.3.5. Selectivity to olefins during the catalyst evolution experiment

We recorded the olefin to paraffin ratios for C_2-C_5 during the dynamic evolution experiment when we were investigating the carburization process of the Co^0, and the result is given in Table 3. The reaction data during the dynamic evolution experiment suggests that similar selectivity to olefins could be achieved with Co^0. In the transient period, when Co is gradually carburized during the first 6 h in this work, there are stages for the catalyst to hold Co^0 only, both Co^0 and Co_2C, and Co_2C only. However, during the former two phases, the selectivity to olefins is similar to the last phase when Co has transformed to Co_2C. Although high selectivity to α-olefins is attributed to the presence of Co_2C as active sites by previous studies [57], while the data here suggests that Co itself could give a comparably high selectivity to α-olefins. This raises the question if Co_2C is essential for a high selectivity to olefins in the FTO. This work suggests that with MnO and Na positioned next, Co^0 can also give a high selectivity to olefins. The DFT calculation (C_2H_4 was used as the representative for olefins in the DFT calculations on metallic Co and various facets for Co_2C) in the literature [26] supports the observation here, although it focused on different Co_2C facets and the result for Co^0 was presented as a reference. The calculation suggests that amongst the various Co_2C facets, on the surface of Co_2C (1 0 1) does the CH_2CH_2 remain the most stable species. While in the meantime, the effective energies for the formation of CH_2CH_2 from two CH_2s on the surface of Co^0 and Co_2C (1 0 1) are very close. It implies that the metallic cobalt favors the formation of olefins similar to some of the Co_2C facets. Still, from a mechanism perspective, it is proven that high selectivity to olefins could be obtained by both Co^0 and Co_2C, supported by the DFT calculation in the literature and the experimental data obtained in this work.

3.3.6. Catalyst stability test

The prepared catalyst was tested for 100 h to demonstrate the stability of its performance. The CO conversion, CH_4, and CO_2 selectivity with time on stream are plotted in Fig. 13, and the O/P ratios for C_2-C_4 HCs are listed in Table 4. The catalyst does not show an apparent deactivation during the 100 h test. The CO conversion dropped slightly but maintained the same level when approaching the end of the test. The O/P ratio for C_2 showed a noticeable drop in the 100 h of the test, while that for C_3 and C_4 are relatively stable. It is well known in the FTS that the hydrogenation ability of C_2H_4 is higher than other olefins. Therefore O/P ratio for C_2 is sensitive to changes in both H_2 partial pressure and the hydrogenation ability of the catalyst. CH_4 selectivity also shows a slight increase during the 100 h test, which could be explained by the same reason that caused the O/P change for C_2.

4. Conclusion

A “melting” catalyst preparation method was adopted to prepare a Co-based catalyst with Mn as a primary promoter and a limited amount of Na as a secondary one. The catalyst prepared by this method for the FTO reaction results in a high selectivity to lower olefins and, in the meantime, low selectivity to CO_2. A very uniform nano-sized Co-Mn composite oxide is manufactured as the precursor catalyst, and Co_2C is

Table 4
Olefin/paraffin ratios for c_2-C_4 during the catalyst stability test.

Reaction time	C_2 O/P	C_3 O/P	C_4 O/P	$C_{2\text{-}4}$O/P
10 h	31.78	15.27	12.98	26.69
30 h	33.95	15.67	16.35	16.35
50 h	28.58	14.14	18.26	18.26
70 h	24.58	15.05	16.29	16.29
100 h	32.82	15.00	15.77	15.77

Reaction conditions: Co/Mn = 2, T = 240 ℃, P = 0.1 MPa(g), H_2/CO = 1, WHSV = 6000 mL/ (h·g_{cat}).

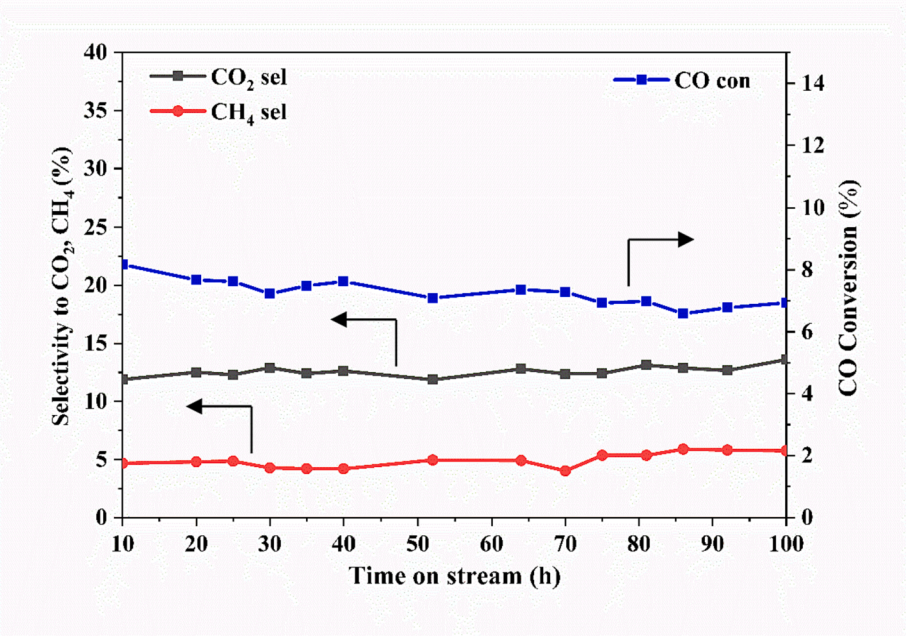

Fig. 13. Stability test for the catalyst (Co/Mn = 2, T = 240 ℃, P = 0.1 MPa(g), H_2/CO = 1, WHSV = 6000 mL/ (h·g_{cat})).

formed by carburization as the catalyst for the FTO reaction. $MnCo_2O_{4.5}$ is identified as the compound for the Co-Mn composite oxide, demonstrating a weak interaction between Co and Mn. Under the H_2 atmosphere, $MnCo_2O_{4.5}$ transforms to metallic Co easily with great reduction extent. Mn is also freed from the composite as MnO that scatters next to the Co. The successful liberation of Co and MnO is due to the presence of Na as $MnCo_2O_{4.5}$ can only be reduced to $Co_xMn_{1-x}O$ instead of Co^0 when no Na is added to the composite. When the reduced catalyst is exposed to syngas at 240 °C, Co_2C is formed via carburization of Co^0, and this process can be finished within 6 h, which is much quicker when compared to some work reported in the literature. Four different crystal facets, (2 1 0), (0 2 0), (1 1 1), and (1 0 1) for Co_2C, are formed under the reaction conditions, and they could be stably maintained with the help of Mn and Na. No converting of Co_2C to Co^0 or further to Co oxides is found during the reaction, but part of Co^0 is oxidized to Co_3O_4 by H_2O formed with the FTO in the course of carburization. At optimal operating conditions, the catalyst achieved 60.26 % selectivity to C_2-C_4 olefins with the O/P ratio in a range of 31.78–12.98 based on the overall HCs produced, 22.70 % selectivity to C_5-C_8 olefins with O/P ratio in a range of 7.73–2.44, while in the meantime the selectivity to CO_2 and CH_4 is 11.49 % and 4.95 %, respectively. With olefins as valuable products, 83.56 % selectivity to C_{2+} hydrocarbons could result in a very high carbon efficiency for the FTO process. Low CO_2 selectivity on the catalyst in this work is believed to be attributed to the high content of Co_2C with no Co-Mn composite oxide left in the active catalyst, the transformation path of how Co_2C is formed via sufficient reduction and carburization, as well as its uniform morphology. The evenly dispersed Na in the catalyst is the key to ensure no remaining Co-Mn composite in the catalyst prepared in this work. Metallic Co formed by reduction for the prepared catalyst is observed to have similarly high olefin to paraffins ratios as Co_2C although it cannot be stably retained under a syngas atmosphere. The stability experiment illustrates that the catalyst is stable within 100 h of the investigation except a drop in the C_2 O/P ratio due to its sensitivity to the change of hydrogenation ability of the catalyst. An increase of Mn content in the catalyst could improve the selectivity to higher olefins (C_5-C_8) but with a price of reduced selectivity to olefins with full carbon spectra.

Declaration of competing interest

The authors declare that they have no known competing financial interests or personal relationships that could have appeared to influence the work reported in this paper.

Data availability

Data will be made available on request.

Acknowledgments

This work is supported by the National Key R&D Program of China (2022YFE0101800) and the Wuhan Institute of Technology (CX-2021037).

Appendix A. Supplementary data

Supplementary data to this article can be found online at https://doi.org/10.1016/j.cej.2023.147927.

References

[1] H.T. Galvis, K.D. Jong, Catalysts for production of lower olefins from synthesis gas: a review, ACS Catal. 3 (2013) 2130–2149.
[2] Q. Zhang, J. Kang, Y. Wang, Development of Novel Catalysts for Fischer-Tropsch Synthesis: Tuning the Product Selectivity, ChemCatChem. 2 (2010) 1030–1058.
[3] J. Bao, G.H. Yang, Y. Yoneyama, N. Tsubaki, Significant Advances in C_1 Catalysis: Highly Efficient Catalysts and Catalytic Reactions, ACS Catal. 9 (2019) 3026–3053.
[4] A.E.M. van den Oever, D. Costa, G. Cardellini, M. Messagie, Systematic Review on the Energy Conversion Efficiency of Biomass-Based Fischer-Tropsch Plants, Fuel. 324 (2022), 124478.
[5] W.X. Peng, S.B. Ge, A.G. Ebadi, H. Hisoriev, M.J. Esfahani, Syngas Production by Catalytic Co-Gasification of Coal-Biomass Blends in a Circulating Fluidized Bed Gasifier, J. Cleaner Prod. 168 (2017) 1513–1517.
[6] J.R. Rostrup-Nielsen, An Industrial Perspective on the Impact of Haldor Topsøe on Research and Development in Synthesis Gas Production, J. Catal. 328 (2015) 5–10.
[7] H.D. Velázquez, R. Cerón-Camacho, M.L. Mosqueira-Mondragón, J.G. Hernández-Cortez, J.A. Montoya-De-La Fuente, M.L. Hernández-Pichardo, T.A. Beltrán-Oviedo, R. Martínez-Palou, Recent Progress on Catalyst Technologies for High Quality Gasoline Production, Catal. Rev. (2022) 1–221.
[8] J.P. Lange, Methanol Synthesis: a Short Review of Technology Improvements, Catal. Today. 64 (2001) 3–8.
[9] P. Tian, Y.X. Wei, M. Ye, Z.M. Liu, Methanol to Olefins (MTO): From Fundamentals to Commercialization, ACS Catal. 5 (2015) 1922–1938.
[10] L.P. Li, Y.Y. Chen, S.T. Xu, J.F. Li, M. Dong, Z.W. Liu, H.J. Jiao, J.G. Wang, W. B. Fan, Oriented Control of Al Locations in the Framework of Al-Ge-ITQ-13 for Catalyzing Methanol Conversion to Propene, J. Catal. 344 (2016) 242–251.
[11] U. Olsbye, S. Svelle, M. Bjørgen, P. Beato, T.V.W. Janssens, F. Joensen, S. Bordiga, K.P. Lillerud, Conversion of Methanol to Hydrocarbons: How Zeolite Cavity and Pore Size Controls Product Selectivity, Angew. Chem., Int. Ed. 51 (2012) 5810–5831.
[12] J. Yang, W.P. Ma, D. Chen, A. Holmen, B.H. Davis, Fischer-Tropsch synthesis: A Review of the Effect of CO Conversion on Methane Selectivity, Appl. Catal. 470 (2014) 250–260.
[13] F. Jiao, J.J. Li, X.L. Pan, J.P. Xiao, H.B. Li, H. Ma, M.M. Wei, Y. Pan, Z.Y. Zhou, M. R. Li, S. Miao, J. Li, Y.F. Zhu, D. Xiao, T. He, J.H. Yang, F. Qi, Q. Fu, X.H. Bao, Selective Conversion of Syngas to Light Olefins, Science. 351 (2016) 1065–1068.
[14] K. Cheng, B. Gu, X.L. Liu, J.C. Kang, Q.H. Zhang, Y. Wang, Direct and Highly Selective Conversion of Synthesis Gas to Lower Olefins: Design of a Bifunctional Catalyst Combining Methanol Synthesis and Carbon-Carbon Coupling, Angew Chem Int Ed Engl. 128 (2016) 4803–4806.
[15] H.M. Torres-Galvis, J.H. Bitter, C.B. Khare, M. Ruitenbeek, A. Dugulan, K. De-Jong, Supported Iron Nanoparticles as Catalysts for Sustainable Production of Lower Olefins, Science. 335 (2012) 835–838.
[16] R. Santen, A.J. Markvoort, I.A.W. Filot, M.M. Ghouri, E.J.M. Hensen, Mechanism and Microkinetics of the Fischer-Tropsch Reaction, Phys. Chem. Chem. Phys. 15 (2013) 17038–17063.
[17] Y. Liu, J.F. Chen, J. Bao, Y. Zhang, Manganese-Modified Fe_3O_4 Microsphere Catalyst with Effective Active Phase of Forming Light Olefins from Syngas, ACS Catal. 5 (2015) 3905–3909.
[18] Y.F. Xu, X.Y. Li, J.H. Gao, J. Wang, G.Y. Ma, X.D. Wen, Y. Yang, Y.W. Li, M.Y. Ding, A hydrophobic FeMn@Si Catalyst Increases Olefins from Syngas by Suppressing C_1 by-Products, Science. 371 (2021) 610–613.
[19] S. Lyu, L. Wang, Z. Li, S.K. Yin, J. Chen, Y.H. Zhang, J.L. Li, Y. Wang, Stabilization of ε-Iron Carbide as High-Temperature Catalyst Under Realistic Fischer-Tropsch Synthesis Conditions, Nat. Commun. 11 (2020) 6219.
[20] Y. Pei, J.X. Liu, Y.H. Zhao, Y.J. Ding, T. Liu, W.D. Dong, H.J. Zhu, H.Y. Su, L. Yan, J.L. Li, W.X. Li, High Alcohols Synthesis via Fischer-Tropsch Reaction at Cobalt Metal/Carbide Interface, ACS Catal. 5 (2015) 3620–3624.
[21] H. Jo, M.K. Khan, M. Irshad, M.W. Arshad, S.K. Kim, J. Kim, Unraveling the Role of Cobalt in the Direct Conversion of CO_2 to High-Yield Liquid Fuels and Lube Base Oil, Appl. Catal. B 305 (2022), 121041.
[22] J.X. Xie, J. Yang, A.I. Dugulan, A. Holmen, D. Chen, K.P. De Jong, M.J. Louwerse, Size and Promoter Effects in Supported Iron Fischer-Tropsch Catalysts: Insights from Experiment and Theory, ACS Catal. 6 (2016) 3147–3157.
[23] J. Gaube, H.F. Klein, The Promoter Effect of Alkali in Fischer-Tropsch Iron and Cobalt Catalysts, Appl. Catal. A 350 (2008) 126–132.
[24] G.R. Johnson, S. Werner, A.T. Bell, An Investigation into the Effects of Mn Promotion on the Activity and Selectivity of Co/SiO_2 for Fischer-Tropsch Synthesis: Evidence for Enhanced CO Adsorption and Dissociation, ACS Catal. 538 (2015) 5888–5903.
[25] C.L. Tucker, Y. Ragoo, S. Mathe, L. Macheli, A. Bordoloi, T.C.R. Rocha, S. Govender, P.J. Kooyman, E. Steen, Manganese Promotion of a Cobalt Fischer-Tropsch Catalyst to Improve Operation at High Conversion, J. Catal. 411 (2022) 97–108.
[26] L.S. Zhong, F. Yu, Y.L. An, Y.H. Zhao, Y.H. Sun, Z.J. Li, T.J. Lin, Y.J. Lin, Q.X. Zhen, Y.Y. Dai, L. Gu, J.S. Hu, S.F. Jin, Q. Shen, H. Wang, Cobalt Carbide Nanoprisms for Direct Production of Lower Olefins from Syngas, Nature. 538 (2016) 84–87.
[27] N.K. Roy, A. Ali, A. Sen, D. Adroja, P. Sen, S.S. Banerjee, Exploring a Low Temperature Glassy State, Exchange Bias Effect, and High Magnetic Anisotropy in Co_2C Nanoparticles, J. Phys.: Condens. Matter. 33 (2021), 375804.
[28] J.C. Mohandas, M.K. Gnanamani, G. Jacobs, W. Ma, Y. Ji, S. Khalid, B.H. Davis, Fischer-Tropsch Synthesis: Characterization and Reaction Testing of Cobalt Carbide, ACS Catal. 1 (2011) 1581–1588.
[29] Y. Liu, D.S. Wu, F. Yu, R.O. Yang, H. Zhang, F.F. Sun, L.S. Zhong, Z. Jiang, *In Situ* XAFS Study on the Formation Process of Cobalt Carbide by Fischer-Tropsch Reaction, Phys. Chem. Chem. Phys. 21 (2019) 10791–10797.
[30] G. Jiao, Y. Ding, H. Zhu, X. Li, J.Y. Li, W. Dong, Y. Pei, Synthesis of Linear Mixed High Alcohols from Syngas over Activated Carbon-Supported Co-Based Catalysts, Chin. J. Catal. 30 (2009) 825–829.
[31] W. Zhou, K. Cheng, J.C. Kang, C. Zhou, V. Subramanian, Q.H. Zhang, Y. Wang, New Horizon in C1 Chemistry: Breaking the Selectivity Limitation in Transformation of Syngas and Hydrogenation of CO2 Into Hydrocarbon Chemicals and Fuels, Chem. Soc. Rev. 48 (2019) 3193–3228.

[32] K. Gong, T.J. Lin, Y.L. An, X.X. Wang, F. Yu, B. Wu, X. Li, S.G. Li, Y.W. Lu, L. S. Zhong, Y.H. Sun, Fischer-Tropsch to Olefins over CoMn-Based Catalysts: Effect of Preparation Methods, Appl. Catal., A. 592 (2020), 117414.
[33] B.J. Wang, D.L. Liang, Z. Guan, D.B. Li, R.G. Zhang, Understanding the Key Step of Co_2C-Catalyzed Fischer-Tropsch Synthesis, J. Phys. Chem. C 124 (2020) 5749–5758.
[34] H. Du, H.J. Zhu, Z. Zhao, W.D. Dong, W.T. Luo, W. Lu, M. Jiang, T. Liu, Y.J. Ding, Effects of Impregnation Strategy on Structure and Performance of Bimetallic CoFe/AC Catalysts for Higher Alcohols Synthesis from Syngas, Appl. Catal., A. 523 (2016) 263–271.
[35] Y.L. An, Y.H. Zhao, Y. Fei, T.J. Lin, Y.W. Lu, S.G. Li, Z.J. Li, Y.Y. Dai, X.X. Wang, H. Wang, L.S. Zhong, Y.H. Sun, Morphology Control of Co_2C Nanostructures via the Reduction Process For Direct Production of Lower Olefins from Syngas, J. Catal. 366 (2018) 289–299.
[36] M. Ao, G.H. Pham, V. Sage, V. Pareek, S.M. Liu, Perovskite-derived trimetallic Co-Ni-Cu catalyst for higher alcohol synthesis from syngas, Fuel Process. Technol. 193 (2019) 141–148.
[37] L. Chen, X.C. Tian, Y.C. Fu, J.Y. Shen, The effect of surface acidic and basic properties of highly loaded Co catalysts on the Fischer-Tropsch synthesis, Catal. Commun. 28 (2012) 155–158.
[38] Q. Zhao, B.B. Chen, J. Li, X.B. Wang, M. Crocker, C. Shi, Insights into the structure-activity relationships of highly efficient CoMn oxides for the low temperature NH3-SCR of Nox, Appl. Catal., B. 277 (2020), 119215.
[39] Z. Gholami, Z. Tisler, R. Velvarska, J. Kocik, CoMn Catalysts Derived from Hydrotalcite-Like Precursors for Direct Conversion of Syngas to Fuel Range Hydrocarbons, Catalysts. 10 (2020) 813.
[40] Z.J. Li, T.J. Lin, F. Yu, Y.L. An, Y.Y. Dai, S.G. Li, L.S. Zhong, H. Wang, P. Gao, Y. H. Sun, M.Y. He, The Mechanism of Mn Promoter via CoMn Spinel for Morphology Control: Formation of Co_2C Nanoprisms for Fischer-Tropsch to Olefins Reaction, ACS Catal. 7 (2017) 8023–8032.
[41] S.N. Zhang, Z.X. Wu, X.F. Liu, Z.L. Shao, L. Xia, L.S. Zhong, H. Wang, Y.H. Sun, Tuning the interaction between Na and Co_2C to promote selective CO_2 hydrogenation to ethanol, Appl. Catal., B. 293 (2021), 120207.
[42] Y.L. An, T.J. Lin, K. Gong, X.X. Wang, L.S. Zhong, H. Wang, Y.H. Sun, Tuning the Facet Proportion of Co_2C Nanoprisms for Fischer-Tropsch Synthesis to Olefins, ChemCatChem. 12 (2020) 1630–1638.
[43] Z. Zhao, W. Lu, R. Yang, H.J. Zhu, W.D. Dong, F.F. Sun, Z. Jiang, Y. Lyu, T. Liu, H. Du, Y.J. Ding, Insight into the Formation of $Co@Co_2C$ Catalysts for Direct Synthesis of Higher Alcohols and Olefins from Syngas, ACS Catal. 8 (2018) 228–241.
[44] H. Lu, L. Schideman, Q. Ye, Y.Q. Lu, High-efficiency catalytic reduction of residual oxygen for purification of carbon dioxide streams from high-pressure oxy-combustion systems, React. Chem. Eng. 6 (2021) 1220–1229.
[45] X.F. Shen, T.F. Zhang, H.Y. Suo, L. Yan, L.C. Huang, C.W. Ma, L.G. Li, X.D. Wen, Y. W. Li, Y. Yang, A Facile One-Pot Method for Synthesis of Single Phase Co_2C With Magnetic Properties, Mater. Lett. 271 (2020), 127783.
[46] N.C. Shiba, X.Y. Liu, H.P. Mao, X.F. Qian, D. Hildebrandt, Y.L. Yao, Effect of Ru-Promotion on the Catalytic Performance of a Cobalt-Based Fischer-Tropsch Catalyst Activated in Syngas or H_2, Fuel. 320 (2022), 123939.
[47] Y. Wang, L.M. Guo, M.Q. Chen, C. Shi, $CoMn_xO_y$ nanosheets with molecular-scale homogeneity: an excellent catalyst for toluene combustion, Catal. Sci. Technol. 8 (2018) 459–471.
[48] S.G. Victoria, A.M.E. Raj, A systematic probe in the properties of spray coated mixed spinel films of cobalt and manganese, J. Phys. Chem. Solids. 112 (2017) 262–269.
[49] S.R. Zhang, J.J. Shan, Y. Zhun, A.L. Frenkel, A. Patlolla, W.X. Huang, S.J. Yoon, L. Wang, H. Yoshida, S. Takeda, F. Tao, WGS Catalysis and *In Situ* Studies of CoO_{1-x}, $PtCo_n/Co_3O_4$, and $Pt_mCo_{m'}/CoO_{1-x}$ Nanorod Catalysts, J. Am. Chem. Soc. 135 (2013) 8283–8293.
[50] Y.Y. Dai, Y.H. Zhao, T.J. Lin, S.G. Li, F. Yu, Y.L. An, X.X. Wang, K. Xiao, F.F. Sun, Z. Jiang, Y.W. Lu, H. Wang, L.S. Zhong, Y.H. Sun, Particle Size Effects of Cobalt Carbide for Fischer-Tropsch to Olefins, ACS Catal. 9 (2019) 798–809.
[51] B. Liu, W.P. Li, Y.B. Xu, Q. Lin, F. Jiang, X.H. Liu, Insight into the Intrinsic Active Site for Selective Production of Light Olefins in Cobalt-Catalyzed Fischer-Tropsch Synthesis, ACS Catal. 9 (2019) 7073–7089.
[52] R.G. Zhang, G.X. Wen, H. Adidharma, A.G. Russell, B.J. Wang, M. Radosz, M. H. Fan, C2 Oxygenate Synthesis via Fischer-Tropsch Synthesis on Co2C and Co/Co2C Interface Catalysts: How to Control the Catalyst Crystal Facet for Optimal Selectivity, ACS Catal. 7 (2017) 8285–8295.
[53] N. Amirov, A.R. Vakhshouri, Numerical Modeling and Optimization of Product Selectivity and Catalyst Activity in Fischer-Tropsch Synthesis via Response Surface Methodology: Cobalt Carbide Particle Size and H_2/CO Ratio Effects, Int. J. Hydrogen Energy. 45 (2020) 31913–31925.
[54] N.C. Shiba, X.Y. Liu, Y.L. Yao, Advances in lower olefin production over cobalt-based catalysts via the Fischer-Tropsch process, Fuel Process. Technol. 238 (2022).
[55] M.H. Zhang, H.P. Yu, Y.Z. Sun, Y.Z. Yu, Y.F. Chen, L.T. Wang, Theoretical and Experimental Insights into CO_2 Formation on Co_2C Catalysts in Syngas Conversion to Value-Added Chemicals, Appl. Surf. Sci. 602 (2022) 15379.
[56] R.Z. Li, Y. Li, Z.H. Li, W.Q. Wei, S.X. Ouyang, H. Yuan, T.R. Zhang, A Metal-Segregation Approach to Generate CoMn Alloy for Enhanced Photothermal Conversion of Syngas to Light Olefins, Sol. RRL. 5 (2020).
[57] N.C. Shiba, Y.L. Yao, X.Y. Liu, D. Hildebrandt, Recent Developments in Catalyst Pretreatment Technologies for Cobalt Based Fisher-Tropsch Synthesis, Rev. Chem. Eng. 38 (2022) 503–538.